HAL
archives-ouvertes.fr

Tropical and subtropical cloud transitions in weather and climate prediction models: The GCSS/WGNE pacific cross-section intercomparison (GPCI)

J. Teixeira, S. Cardoso, M. Bonazzola, J. Cole, A. Delgenio, C. Demott, C. Franklin, C. Hannay, C. Jakob, Y. Jiao, et al.

▶ **To cite this version:**

J. Teixeira, S. Cardoso, M. Bonazzola, J. Cole, A. Delgenio, et al.. Tropical and subtropical cloud transitions in weather and climate prediction models: The GCSS/WGNE pacific cross-section intercomparison (GPCI). Journal of Climate, American Meteorological Society, 2011, 24 (20), pp.5223-5256. <10.1175/2011jcli3672.1>. <hal-01132266>

HAL Id: hal-01132266

https://hal.archives-ouvertes.fr/hal-01132266

Submitted on 17 Mar 2015

HAL is a multi-disciplinary open access archive for the deposit and dissemination of scientific research documents, whether they are published or not. The documents may come from teaching and research institutions in France or abroad, or from public or private research centers.

L'archive ouverte pluridisciplinaire **HAL**, est destinée au dépôt et à la diffusion de documents scientifiques de niveau recherche, publiés ou non, émanant des établissements d'enseignement et de recherche français ou étrangers, des laboratoires publics ou privés.

Tropical and Subtropical Cloud Transitions in Weather and Climate Prediction Models: The GCSS/WGNE Pacific Cross-Section Intercomparison (GPCI)

J. TEIXEIRA,[a] S. CARDOSO,[b,c] M. BONAZZOLA,[d] J. COLE,[e] A. DELGENIO,[f] C. DEMOTT,[g] C. FRANKLIN,[h] C. HANNAY,[c] C. JAKOB,[i] Y. JIAO,[j] J. KARLSSON,[k] H. KITAGAWA,[l] M. KÖHLER,[m] A. KUWANO-YOSHIDA,[n] C. LEDRIAN,[o] J. LI,[a] A. LOCK,[p] M. J. MILLER,[m] P. MARQUET,[q] J. MARTINS,[b] C. R. MECHOSO,[r] E. V. MEIJGAARD,[s] I. MEINKE,[t] P. M. A. MIRANDA,[b] D. MIRONOV,[u] R. NEGGERS,[s] H. L. PAN,[v] D. A. RANDALL,[g] P. J. RASCH,[w] B. ROCKEL,[x] W. B. ROSSOW,[y] B. RITTER,[u] A. P. SIEBESMA,[s] P. M. M. SOARES,[b] F. J. TURK,[a] P. A. VAILLANCOURT,[z] A. VON ENGELN,[aa] AND M. ZHAO[bb]

[a] *Jet Propulsion Laboratory, California Institute of Technology, Pasadena, California*
[b] *Instituto Dom Luis, University of Lisbon, Lisbon, Portugal*
[c] *National Center for Atmospheric Research, Boulder, Colorado*
[d] *Laboratoire de Météorologie Dynamique, Paris, France*
[e] *Canadian Centre for Climate Modelling and Analysis, Victoria, British Columbia, Canada*
[f] *NASA Goddard Institute for Space Studies, New York, New York*
[g] *Department of Atmospheric Science, Colorado State University, Fort Collins, Colorado*
[h] *Centre for Australian Weather and Climate Research, Melbourne, Victoria, Australia*
[i] *Monash University, Melbourne, Victoria, Australia*
[j] *Department of Earth and Atmospheric Sciences, Université du Québec à Montréal, Montreal, Quebec, Canada*
[k] *Stockholm University, Stockholm, Sweden*
[l] *Japan Meteorological Agency, Tokyo, Japan*
[m] *European Center for Medium-Range Weather Forecasts, Reading, United Kingdom*
[n] *Computational Earth Science Research Program, Earth Simulator Center, Japan Agency for Marine-Earth Science and Technology, Yokohama, Japan*
[o] *Institute for Atmospheric and Climate Science, Eidgenössische Technische Hochschule Zentrum, Zürich, Switzerland*
[p] *United Kingdom Meteorological Office, Exeter, United Kingdom*
[q] *Météo-France, Centre National de Recherches Meteorologiques, Toulouse, France*
[r] *Department of Atmospheric and Oceanic Sciences, University of California, Los Angeles, Los Angeles, California*
[s] *Koninklijk Nederlands Meteorologisch Instituut, De Bilt, The Netherlands*
[t] *Experimental Climate Prediction Center, University of California, San Diego, La Jolla, California*
[u] *Research and Development Division, Deutscher Wetterdienst, Offenbach, Germany*
[v] *Environmental Modeling Center, National Centers for Environmental Prediction, Camp Springs, Maryland*
[w] *Pacific Northwest National Laboratory, Richland, Washington*
[x] *Institute for Coastal Research, GKSS Research Centre, Geesthacht, Germany*
[y] *CREST, The City College of New York, New York, New York*
[z] *Recherche en Prévision Numérique, Canadian Meteorological Centre, Environment Canada, Dorval, Quebec, Canada*
[aa] *EUMETSAT, Darmstadt, Germany*
[bb] *Geophysical Fluid Dynamics Laboratory, Princeton, New Jersey*

(Manuscript received 11 February 2010, in final form 4 January 2011)

Corresponding author address: J. Teixeira, Jet Propulsion Laboratory, 4800 Oak Grove Dr., Pasadena, CA 91109.
E-mail: joao.teixeira@jpl.nasa.gov

DOI: 10.1175/2011JCLI3672.1

© 2011 American Meteorological Society

ABSTRACT

A model evaluation approach is proposed in which weather and climate prediction models are analyzed along a Pacific Ocean cross section, from the stratocumulus regions off the coast of California, across the shallow convection dominated trade winds, to the deep convection regions of the ITCZ—the Global Energy and Water Cycle Experiment Cloud System Study/Working Group on Numerical Experimentation (GCSS/WGNE) Pacific Cross-Section Intercomparison (GPCI). The main goal of GPCI is to evaluate and help understand and improve the representation of tropical and subtropical cloud processes in weather and climate prediction models. In this paper, a detailed analysis of cloud regime transitions along the cross section from the subtropics to the tropics for the season June–July–August of 1998 is presented. This GPCI study confirms many of the typical weather and climate prediction model problems in the representation of clouds: underestimation of clouds in the stratocumulus regime by most models with the corresponding consequences in terms of shortwave radiation biases; overestimation of clouds by the 40-yr ECMWF Re-Analysis (ERA-40) in the deep tropics (in particular) with the corresponding impact in the outgoing longwave radiation; large spread between the different models in terms of cloud cover, liquid water path and shortwave radiation; significant differences between the models in terms of vertical cross sections of cloud properties (in particular), vertical velocity, and relative humidity. An alternative analysis of cloud cover mean statistics is proposed where sharp gradients in cloud cover along the GPCI transect are taken into account. This analysis shows that the negative cloud bias of some models and ERA-40 in the stratocumulus regions [as compared to the first International Satellite Cloud Climatology Project (ISCCP)] is associated not only with lower values of cloud cover in these regimes, but also with a stratocumulus-to-cumulus transition that occurs too early along the trade wind Lagrangian trajectory. Histograms of cloud cover along the cross section differ significantly between models. Some models exhibit a quasi-bimodal structure with cloud cover being either very large (close to 100%) or very small, while other models show a more continuous transition. The ISCCP observations suggest that reality is in-between these two extreme examples. These different patterns reflect the diverse nature of the cloud, boundary layer, and convection parameterizations in the participating weather and climate prediction models.

1. Introduction

By the end of World War II there were 22 weather ships stationed in the Atlantic Ocean and 24 in the Pacific Ocean.[1] From July to October 1945, three weather ships were stationed in a Pacific transect from San Francisco to Honolulu and were able to sample in a fairly continuous manner the weather conditions in a region where important climatic cloud transitions occur from stratocumulus regimes (off the coast of California) to cumulus regimes close to Hawaii. The observations collected by these ships along this Pacific Ocean transect allowed, for the first time, construction of a detailed view of the three-dimensional structure of this key subtropical boundary layer transition as the atmosphere is advected over warmer waters (and lower subsidence) along the trade winds (Riehl et al. 1951).

Along similar transects, the stratocumulus cloud decks, which typically overlay the cold waters off the west coast of continents, transition to shallow cumulus topped boundary layers (e.g., Albrecht et al. 1995; Bretherton et al. 1999) and then eventually to deep cumulus convection over the warmer waters of the intertropical convergence zone. The cloud regimes, associated with the boundary layer, deep convection, and the transitions between them, play a significant role in modulating the tropical and subtropical atmospheric circulation and are known to have a profound influence on the physics and dynamics of climate (e.g., Philander et al. 1996; Ma et al. 1996; Larson et al. 1999). In climate change sensitivity experiments (e.g., doubling CO_2), current climate models display profoundly different responses in terms of boundary layer (low) clouds, often leading to cloud–climate feedbacks of opposing signal (e.g., Bony et al. 2004, 2006; Bony and Dufresne 2005; Wyant et al. 2006; Stephens 2005). It is tenable that changes in the characteristics of the stratocumulus to cumulus transition play an important role in cloud–climate feedbacks.

Unfortunately, many of the important characteristics of these cloud regimes are not realistically represented in weather and climate prediction models (e.g., Jakob 1999; Duynkerke and Teixeira 2001; Siebesma et al. 2004). This is in spite of some promising advances in the development of cloud and cloudy boundary layer parameterizations during the last several years (e.g., Tiedtke 1993; Del Genio et al. 1996; Fowler et al. 1996; Rasch and Kristjánsson 1998; Lock et al. 2000; Lock 2001; Bony and Emanuel 2001; Teixeira and Hogan 2002; Tompkins 2002).

The need to better understand the physics and dynamics of clouds and to improve the parameterizations of clouds and cloud-related processes in weather and climate prediction models led to the creation of the

[1] After the war 13 weather ships remained in the Atlantic and Pacific until 1980.

Global Energy and Water Cycle Experiment (GEWEX) Cloud Systems Study (GCSS) in the early 1990s (Browning et al. 1993; Randall et al. 2003). The research efforts in GCSS have been divided into different cloud types (boundary layer clouds, cirrus, frontal clouds, deep convection, and polar clouds) and have extensively used large-eddy simulation (LES) and cloud-resolving models (CRM) to assess and develop parameterizations for single-column models (SCM), which are one-dimensional versions of weather and climate prediction models.

The traditional GCSS strategy can be divided in the following steps: (i) create a case study using observations; (ii) evaluate CRM/LES models for the case study; (iii) use SCMs to evaluate the parameterizations; and (iv) use the statistics from CRM/LES to develop and improve parameterizations. This strategy has been quite successful in improving CRM/LES models, in helping to define and understand fundamental cloud regimes (e.g., Duynkerke et al. 1999; Bretherton et al. 1999; Bechtold et al. 2000; Redelsperger et al. 2000; Stevens et al. 2001; Randall et al. 2003; Siebesma et al. 2003) and in developing new parameterizations for clouds and the cloudy boundary layer (e.g., Cuijpers and Bechtold 1995; Lock et al. 2000; Golaz et al. 2002; Teixeira and Hogan 2002; Cheinet and Teixeira 2003; Lenderink and Holtslag 2004; Bretherton et al. 2004; Soares et al. 2004; Bretherton and Park 2009).

2. GCSS/WGNE Pacific cross-section intercomparison

a. Introduction

Despite its successes, the current GCSS strategy of using only one-dimensional subsets (SCMs) of weather and climate prediction models falls short of addressing the fundamental role of clouds in climate since it does not allow for feedback to the large-scale dynamics. The latter can only be achieved by using fully three-dimensional models of the atmosphere. In turn, the analysis of such models is notoriously difficult owing to the large amount of information required for meaningful conclusions to be drawn.

In this paper, a model evaluation strategy is adopted in which weather and climate prediction models are analyzed along a cross section in the Pacific Ocean, from the coast of California to the equatorial region, as illustrated in Fig. 1. The figure also depicts the low (boundary layer) cloud cover climatology from the International Satellite Cloud Climatology Project (ISCCP) (Rossow and Schiffer 1999) for the June–July–August (JJA) season. This approach aims at complementing the more traditional efforts in GCSS by providing a simple framework for the evaluation of weather and climate prediction models

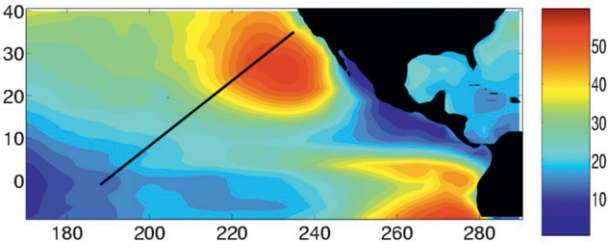

FIG. 1. The GCSS/WGNE Pacific cross section, from the stratocumulus regions off the west coast of California, across the trade cumulus regions, to the equator together with the ISCCP low cloud cover (%) climatology for the June–July–August season.

that encompasses several fundamental cloud regimes, such as stratocumulus, shallow cumulus, and deep cumulus, as well as the transitions between them. The fact that data is only needed along a model transect allows for a technically less involved intercomparison.

The overall goal is to use the GPCI framework to understand cloud regimes and regime transitions in the tropics and subtropics and to characterize the main deficiencies in climate models in terms of the representation of clouds and cloud-related processes. These analyses should lead to the development of new parameterizations of clouds, boundary layer, and convection and consequently contribute to more accurate predictions of climate change. Ultimately, it is the combination of the model and the satellite data and the use of new analysis techniques that will improve our ability to not only establish the model shortcomings but also to gain insight in the physical reasons leading to these deficiencies.

Preliminary studies using a similar cross section across the Pacific Ocean were performed in the context of a European Cloud Systems Study (EUROCS). While important, the EUROCS results (Siebesma et al. 2004) were limited due to coarse temporal resolution (only monthly mean values at four different times per day were available) and the absence of some critical observational data sources for the evaluation of the model results, such as information about the tropospheric temperature and humidity structure.

As a summary, the main general motivations for GPCI are

- to study important cloud regimes and transitions—stratocumulus, shallow cumulus, and deep convection;
- to evaluate models and observations in the tropics and subtropics in terms of the atmospheric hydrologic cycle;
- to utilize a new generation of satellite datasets;
- to help the development of new cloud, convection, and turbulence parameterizations in weather and climate models;

- to include 3D weather and climate models in the GCSS framework; and
- to create a database of models and observations for future studies of the tropics and subtropics.

b. Model data

Model output from over 20 weather and climate prediction organizations was collected and organized for GPCI (see appendix A and Tables A1 and A2 therein for more information). The three-hourly model output from simulations of the periods of June–July–August 1998 and 2003 (only 1998 results are discussed in this paper) is produced for 13 points along the GPCI transect from 35°N, 125°W in the northeast to 1°S, 173°W in the southwest (see appendix B for details on the GPCI specifications—in particular, the locations of the points). A three-hourly model output frequency permits better characterization of the diurnal variability and provides the opportunity of applying novel model evaluation techniques. These types of analyses were unavailable during the EUROCS study (Siebesma et al. 2004) because of the temporally sparse data sampling.

c. Satellite data

In the context of GPCI, model results are evaluated against a variety of satellite observations. Satellite observations have been for some time a fundamental tool for our understanding of the role of clouds in the climate system (e.g., Ramanathan et al. 1989; Harrison et al. 1990; Rossow and Schiffer 1991, 1999; Wielicki et al. 1995; Chylek et al. 2007) and for the evaluation of climate and weather prediction models (e.g., Cess et al. 1997; Webb et al. 2001; Randall et al. 2003; Zhang et al. 2005). The high vertical and temporal resolution of the GPCI model data will facilitate a more complete utilization of satellite data.

A collection of satellite data related to GPCI is available online at the GCSS Data Integration for Model Evaluation (DIME) Web site (http://gcss-dime.giss.nasa.gov/). These datasets include high temporal resolution data from the International Satellite Cloud Climatology Project (ISCCP) together with daily products from the Special Sensor Microwave Imager (SSM/I), the Global Precipitation Climatology Project (GPCP), and the TIROS Operational Vertical Sounder (TOVS). For more details on the satellite data see appendix C. In this manuscript the potential of the ISCCP data for the study of cloud regime transitions is explored in detail. Note, that when using the ISCCP simulator (Klein and Jakob 1999; Webb et al. 2001) it is often possible to extract more information from a comparison between models and ISCCP observations. Unfortunately, many of the models used in the GPCI exercise do not have the ISCCP simulator implemented. To make this intercomparison as inclusive and simple as possible no ISCCP simulator output was requested.

d. Two-dimensional data

It can be argued that a single cross section may miss key physical events that occur in a certain region. For example, when analyzing the diurnal cycle over the stratocumulus regions, it must be taken into account that subsidence may be caused by convection somewhere over land, which may not be present in the cross section. To tackle these types of problems without requiring vast amounts of three dimensional data, GPCI requested output [of only a few variables such as outgoing longwave radiation (OLR) or precipitation, for example] in a two-dimensional region that contains the cross section (5°S–45°N, 160°E–120°W).

3. How representative is the GPCI transect?

The first obvious question regarding this study is: how representative is the GPCI transect in the sense of capturing the most relevant physical processes of this region of the subtropical and tropical Pacific?

In this section two types of results are shown so as to address this question. First, the wind direction at 1000 and 900 hPa along the GPCI cross section from the 40-yr ECMWF Re-Analysis (ERA-40) product (Uppala et al. 2005) is analyzed. Figures 2 and 3 show histograms of wind direction at 900 and 1000 hPa, respectively, for six points along the GPCI transect for June–July–August (JJA) 1998. These figures illustrate how, for (at least) the points from 8° to 26°N (at 1000 hPa), and from 14° to 26°N (at 900 hPa), the wind direction histograms are reasonably parallel to the GPCI transect. These results confirm that, at least for ERA-40, the orientation of the GPCI transect is close to the mean boundary-layer trade wind trajectories. This may well not be exactly the case for some of the models, but as will be shown later, all models exhibit characteristics of a Hadley circulation in this region, suggesting that the model boundary layer trajectories do not diverge profoundly from the ERA-40 results.

The 2D dataset mentioned above is used so as to investigate how representative histograms of variables, like total cloud cover (TCC) and precipitation, are along the GPCI transect compared to longitudinally adjacent points (5 degrees to the east and to the west). Figure 4 shows the histograms of precipitation for one GPCI point (5°N, 195°E) and the two adjacent points from the GFDL, and NCAR models for the period of June–July–August 1998. Figure 5 shows a similar plot but for the TCC and another GPCI point—20°N, 215°E. It is clear from these figures that the histograms for both TCC and precipitation

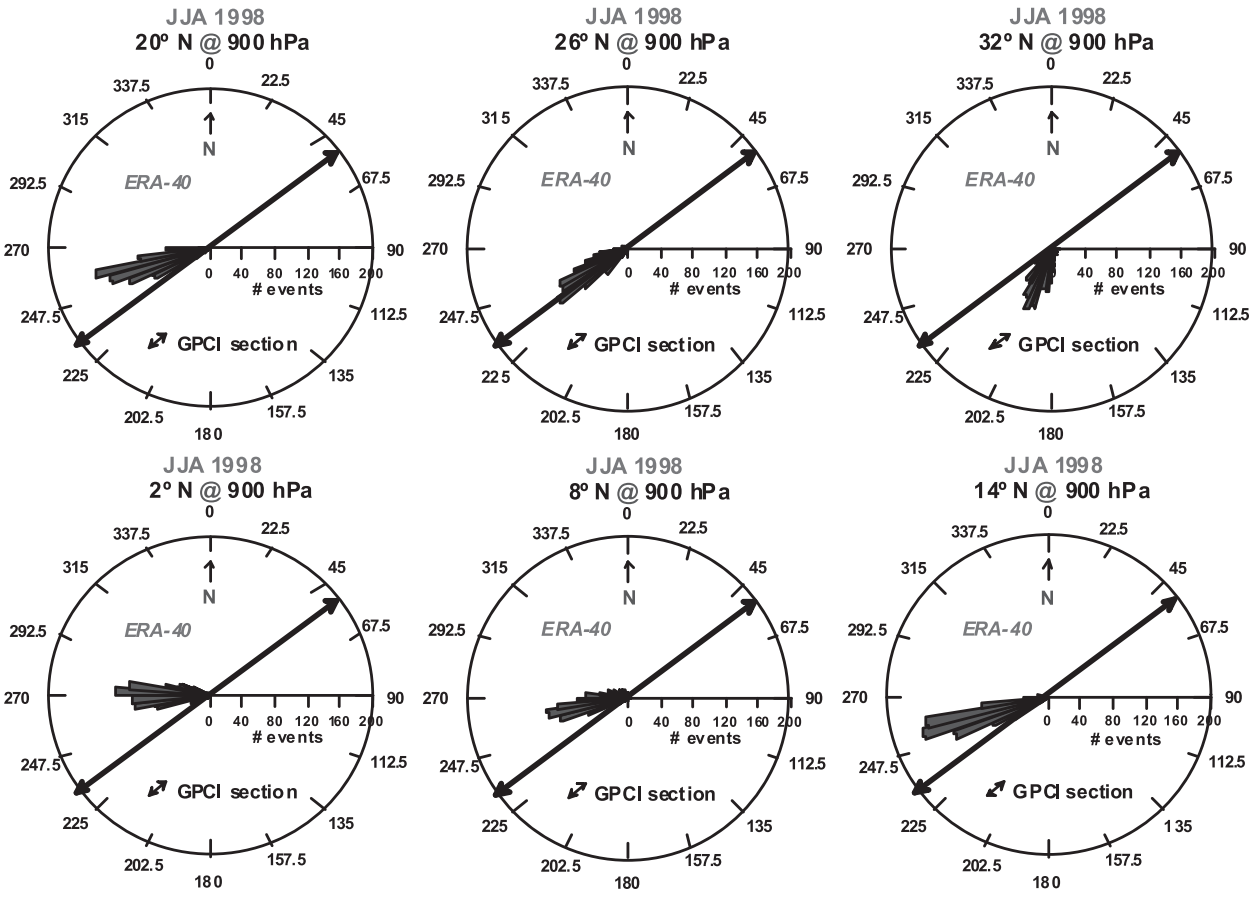

FIG. 2. Histograms of wind direction at 900 hPa for six points along the GPCI transect from ERA-40 (June–July–August 1998).

are quite similar between adjacent points for the same model and quite different between models. Similar results are obtained for different points along the GPCI transect as well as for different models (not shown). Overall, these results support the idea that GPCI is sufficiently representative for the purposes of this study of the main model physical processes of the subtropics in this region.

4. Mean single-level parameter results

In this and the following subsections several results will be analyzed. The results shown correspond to June–July–August 1998. The sea surface temperature (SST) boundary condition is prescribed in virtually all of the models (the exception being the NCEP coupled ocean–atmosphere version] but following slightly independent implementation techniques (e.g., different SST analysis). Figure 6 shows the June–July–August 1998 mean SST prescribed (or obtained, in the case of the coupled system) for each of the model simulations along the GPCI transect. Although using slightly different implementations for describing SST, all of the (uncoupled) models show similar SST distributions along the GPCI transect. The SSTs increase almost linearly southward from the cold waters (~290 K) off the coast of California and peak in the ITCZ region (~302 K). The SST from the NCEP coupled simulation [NCEP GFS and MOM3 (G&M3) in the figure] is warmer in the subtropical regions, associated (at least partly) with a negative cloud bias. We will return to this important feedback between low clouds and the SST.

Figure 7a shows the ensemble (composed of the different models) model mean and the across-model variability of total column water vapor (TWV) along the GPCI transect for JJA 1998. The across-model variability is characterized by the ensemble mean plus or minus the standard deviation and by the maximum and minimum values attained by any of the models (range) for a particular GPCI-transect point. Also shown are the results from ERA-40 and the SSM/I observations. The increase of TWV from the stratocumulus regions off California toward the ITCZ follows the increase in SST. According to SSM/I, the TWV increases from around 18 kg m^{-2} close to the California coast (35°N) to just over 50 kg m^{-2} over the ITCZ. This illustrates well the major changes that

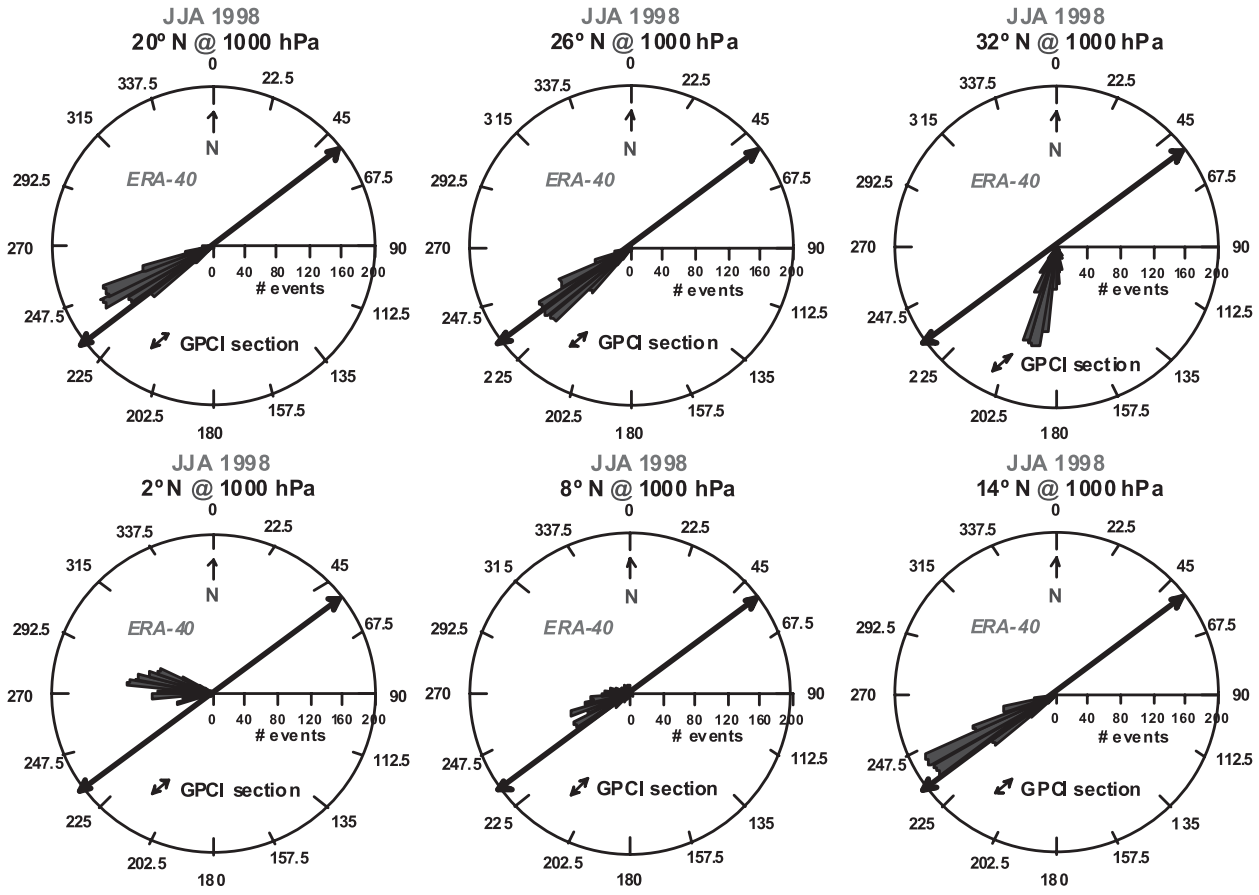

FIG. 3. As in Fig. 2, but at 1000 hPa.

occur in the atmospheric column as it transitions from a situation with a shallow boundary layer, capped by a dry upper troposphere, to a situation with fully developed deep moist convection events.

TWV is an integral parameter that is fundamental in characterizing the atmospheric hydrologic cycle. In this context, the good agreement between SSM/I and ERA-40 is worthy of notice. If these observations and analyses were to differ in any significant manner in terms of this key parameter, this would mean that there were some serious deficiencies in either or both of these datasets. Fortunately this is not the case. Of course, since ERA-40 assimilates observations such as (or of the type of) SSM/I, it could still be argued that these similarities are to be expected. In general, these results suggest that ERA-40 is reproducing well this integral parameter in terms of the hydrologic cycle. On the other hand, as will be amply discussed in this paper, ERA-40 still suffers from deficiencies in many variables and this type of agreement between ERA-40 and the observations is not so common for other parameters.

Many of the models exhibit a behavior, in terms of TWV, that is not substantially different from the one obtained with SSM/I or ERA-40. This is not necessarily surprising given the integral nature of TWV. Some models, however, do show noticeable departures from SSM/I and ERA-40 (in some, or even all, of the locations along the GPCI transect). Because TWV is an integral measure of the atmospheric water vapor content, the across-model standard deviation looks relatively small when compared to other variables, but the minimum and maximum values are of concern. In the stratocumulus regions, the difference between the maximum and minimum values is of the same order of magnitude as the measured TWV. These differences in terms of TWV are often associated with differences in boundary layer height. Boundary layer height is a key parameter in characterizing the cloudy boundary layer structure and, as will be discussed below, the models produce a variety of behaviors leading to significant differences in terms of clouds and boundary layer height (e.g., Karlsson et al. 2010). In the deep tropics the difference between maximum and minimum values is $O(20\ \mathrm{kg\ m^{-2}})$.

The simulated and observed (ISCCP) total cloud cover (TCC) along the GPCI transect is shown in Fig. 7b. Immediately obvious, when compared with TWV, is the

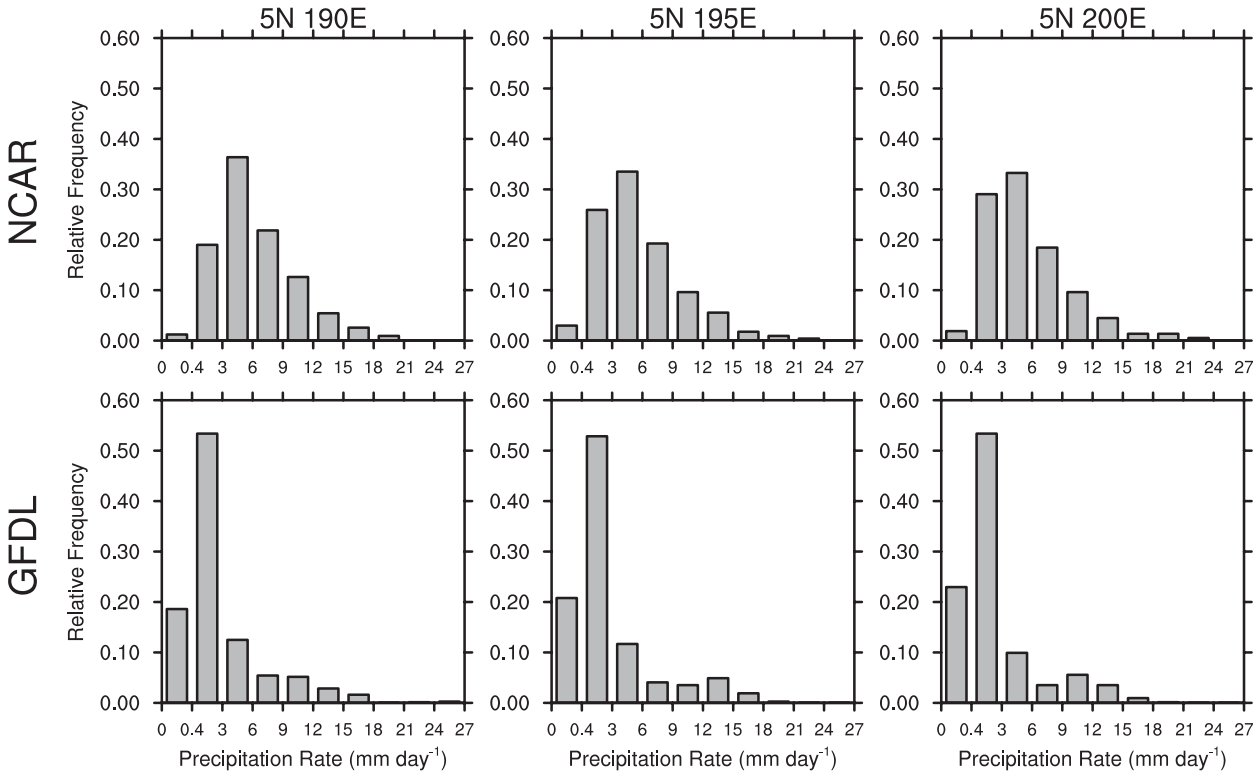

FIG. 4. Histogram of precipitation (mm day^{-1}) from the NCAR and GFDL models for one GPCI point (5°N, 195°E) and two adjacent (5° to the east and west along the same latitude) points for June–July–August 1998.

degree of scatter of the results. From this plot alone it is quite clear that weather and climate prediction models have serious problems simulating clouds. Note that, as opposed to TWV (as discussed above), ERA-40 diverges substantially from ISCCP. Although ISCCP observations still have significant uncertainties, in particular ISCCP TCC in the tropics is an underestimate by 10%–15% because of very thin cirrus that are not detected (e.g., Stubenrauch et al. 1999), it is fair to argue that at this stage of current understanding, the ISCCP cloud cover product is more trustworthy than ERA-40, which is an analysis that assimilates virtually no explicit cloud information. In particular, ERA-40 underestimates TCC in the stratocumulus (and initial transition to cumulus) region, between 23° and 35°N and overestimates TCC in the ITCZ region. This negative TCC bias in the stratocumulus regions was much more pronounced in ERA-15, the previous version of the reanalysis (Duynkerke and Teixeira 2001), but has been ameliorated with subsequent model improvements, namely increased vertical resolution in the boundary layer (Teixeira 1999). ERA-Interim, the most recent ECWMF version of the reanalysis, has shown significant additional improvements of the simulations of marine low clouds due to the implementation of the eddy-diffusivity mass-flux approach, originally proposed by Siebesma and Teixeira (2000), focused on the stratocumulus regime (Köhler 2005; Hannay et al. 2009).

The models in general, as can be seen by the ensemble mean, still underestimate TCC in the stratocumulus regions—a negative bias of around 20%–30% compared to ISCCP. Some models produce extremely low values of TCC in regions typically associated with stratocumulus and where ISCCP TCC is large. However, there are a few models that manage to simulate stratocumulus TCC in a relatively accurate manner. In the trade cumulus regions between 14° and 20°N the ensemble mean shows good agreement with ERA-40 and ISCCP. In the ITCZ region the ensemble model mean is reasonably close to ISCCP, while ERA-40 overestimates TCC by as much as 20% (note, however, the possible ISCCP negative bias in the deep tropics mentioned above). The standard deviation and range between maximum and minimum values of TCC in this region are also quite large. Overall the TCC across-model variability (standard deviation and range) is uncomfortably large throughout the entire GPCI transect: the difference between the maximum and minimum values is always larger than 50% cloud cover.

It is important to note that sometimes in the plots being shown the maximum and minimum values are associated with models that are clearly underperforming when

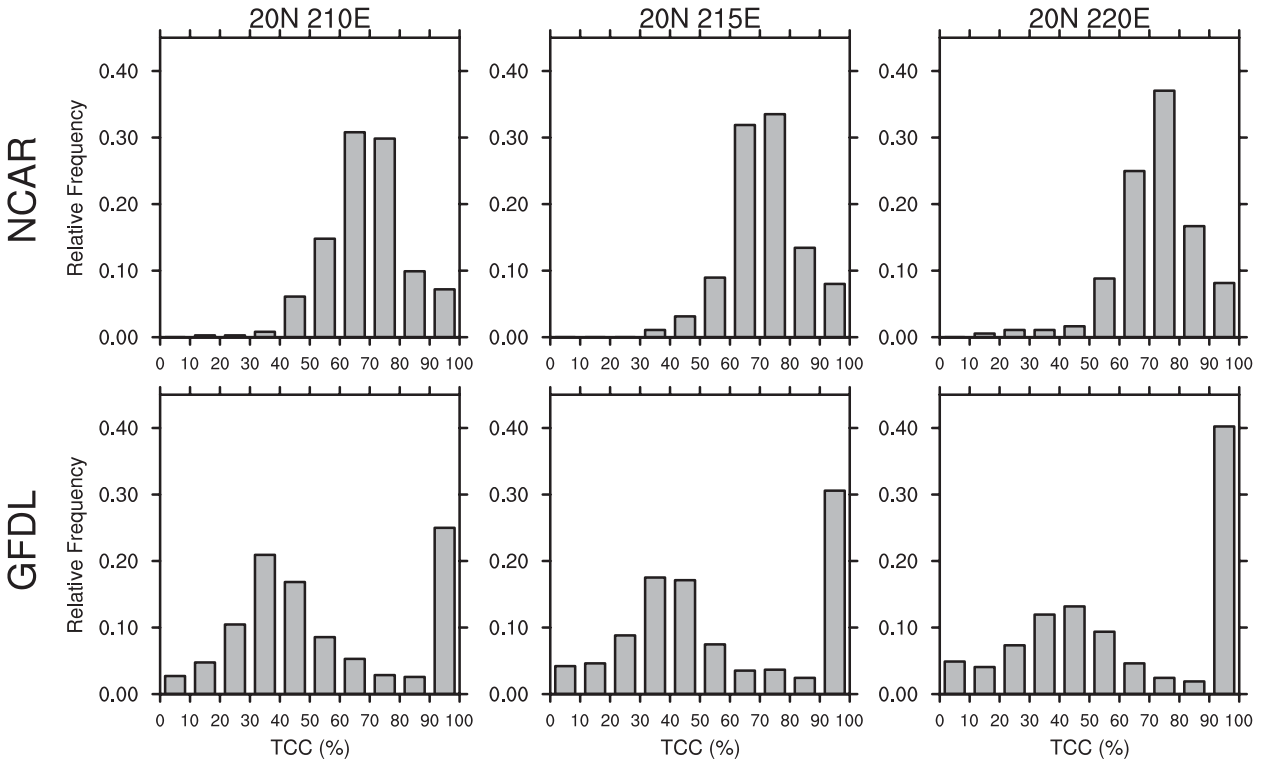

FIG. 5. Histogram of total cloud cover (TCC) (%) from the NCAR and GFDL models for one GPCI point (20°N, 215°E) and two adjacent (5° to the east and west along the same latitude) points for June–July–August 1998.

compared with most models for that particular variable. However, except for situations in which a particular model produces values that are unphysical or clearly divergent from all the other models, we opt for including all models in the statistics. On the other hand, the range between models in variables like TCC is physically significant (not necessarily in a purely statistical sense) and should be interpreted as a serious problem of weather and climate prediction models in general. The reader interested in analyzing the data from a particular model is advised to go to the GPCI/DIME Web site (http://gcss-dime.giss.nasa.gov/gpci/modsim_gpci_models.html).

Figure 7c shows the equivalent figure but for the liquid water path (LWP) with observations from SSM/I. It is clear that both ERA-40 and the ensemble model mean underestimate LWP in the stratocumulus regions, while ERA-40 (but not the ensemble mean) overestimates LWP values over the trade cumulus regions. Over the deep tropics ERA-40 clearly overestimates LWP as compared with SSM/I, with a peak of around 350 g m^{-2} versus an observed peak of about 200 g m^{-2}, while the ensemble mean is relatively close to the observations.

It must be noted that LWP observations from microwave instruments such as SSM/I can have significant uncertainties (see Li et al. 2008, for a comparison between different satellite observations of LWP). The results shown in Fig. 7c are, however, consistent with the overall picture of an underestimation of clouds from ERA-40 and the ensemble mean over the stratocumulus regions and an overestimation of ERA-40 over the ITCZ. More recent observations such as from *CloudSat* (e.g., Stephens et al. 2002) may help clarify some of the observational issues and narrow down the observational uncertainties. A remarkable characteristic of the model results is again

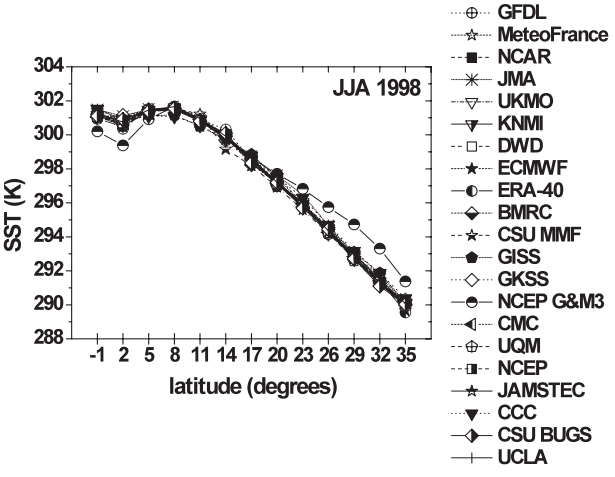

FIG. 6. Sea surface temperature (SST) along GPCI for June–July–August 1998.

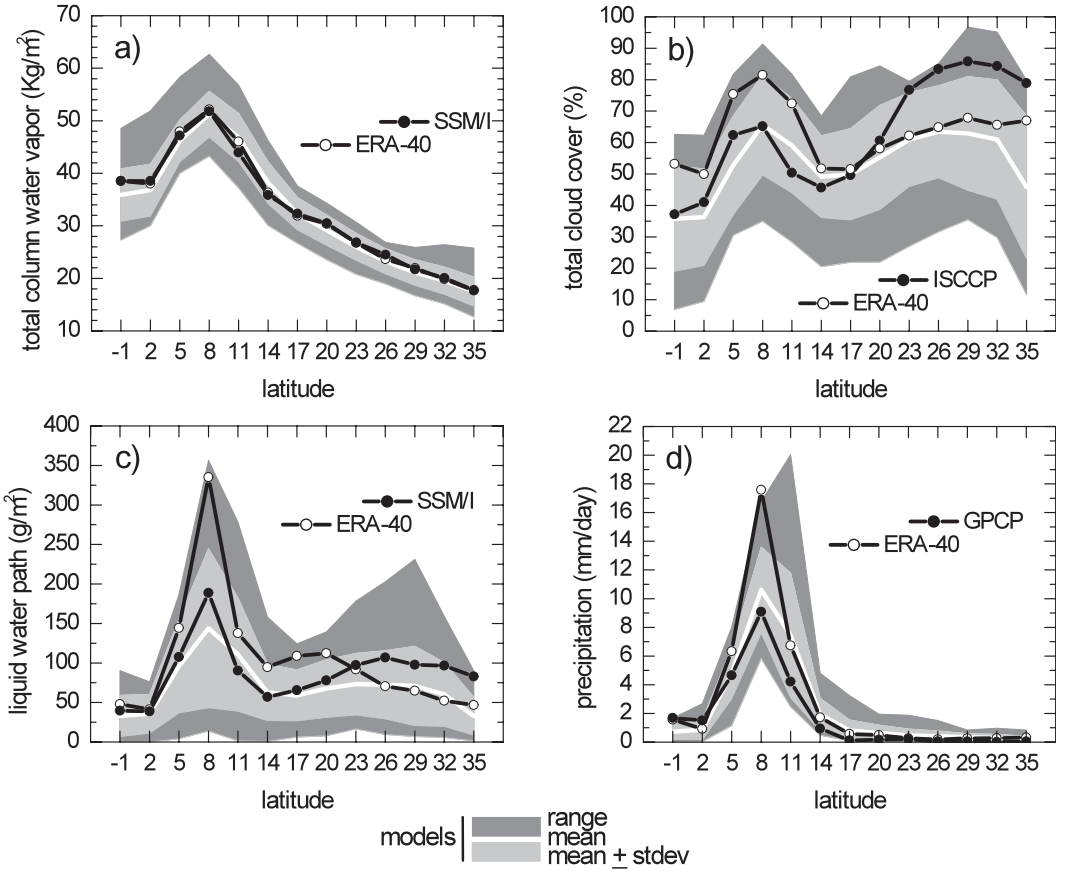

FIG. 7. (a) Total column water vapor from the models along GPCI for JJA 1998 together with ERA-40 and SSM/I, (b) as in (a) but for total cloud cover and ISCCP observations, (c) as in (a) but for liquid water path, and (d) as in (a) but for precipitation and GPCP observations. Results from the different models are shown as ensemble mean results, the mean plus or minus the standard deviation, and the maximum and minimum values attained by any model for a particular point (referred to as range).

their large across-model variability. The LWP minimum and mean minus one standard deviation are extremely low throughout the transect, illustrating well the difficulties that climate and weather prediction models have in representing boundary layer clouds in a realistic way.

Figure 7d is the equivalent figure for precipitation with GPCP observations. This figure illustrates well a key difference between the subtropical regions dominated by boundary layer clouds and the ITCZ dominated by deep convection. In models and observations the subtropics are characterized by modest (or virtually absent) amounts of precipitation, with the exception of the model maximum value, showing that at least one model produces precipitation close to 2 mm day^{-1} in the trade cumulus regions. Note that accurate observations of precipitation in these relatively dry regions are hard to obtain (e.g., Adler et al. 2003), and we should consider that the error bars associated with GPCP in these regions are relatively large (percentwise) (e.g., Janowiak et al. 1998). Over the ITCZ, GPCP shows mean June–July–August 1998 values of around 9 mm day^{-1} slightly below the model ensemble mean. ERA-40, on the other hand, produces values slightly above the maximum value of all the models and about twice as estimated by GPCP; again, an overactive ERA-40 in the deep tropics is apparent.

The outgoing longwave radiation (OLR) results are shown in Fig. 8a with observations from CERES. Over the subtropical regions dominated by boundary layer clouds topped by a dry free troposphere, the OLR CERES observations lie in-between the model ensemble mean values (lower than the observations) and ERA-40 (higher than the observations). In the deep convective regions ERA-40 underestimates the OLR, when compared with CERES data, producing a bias of around 20 W m^{-2}, while the ensemble mean follows the CERES observations quite closely. An underestimation of OLR in ERA-40 for the ITCZ is consistent with positive ERA-40 biases of LWP, precipitation, and TCC.

The equivalent figure for the net shortwave radiative flux at the top of the atmosphere (SW at TOA) is shown

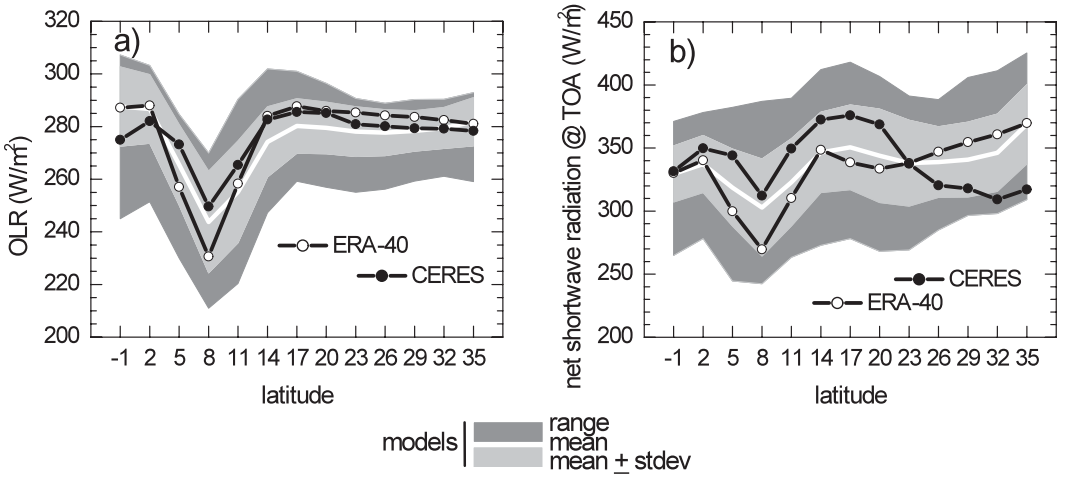

FIG. 8. (a) Outgoing longwave radiation (OLR) from the models along GPCI for June–July–August 1998 together with ERA-40 and CERES, (b) as in (a) but for net shortwave radiation at the TOA and CERES observations. Results from the different models are shown as ensemble mean results, the mean plus or minus the standard deviation, and the maximum and minimum values attained by any model for a particular point (referred to as range).

in Fig. 8b, with observations from CERES. The results of net SW at TOA from ERA-40 and from the ensemble mean are relatively similar in the subtropical regions. Over the stratocumulus areas both ERA-40 and the ensemble mean overestimate the net SW at TOA by up to 50 W m^{-2} on the mean, reflecting a negative bias in terms of cloud cover and cloud water. Over the Cu regions ERA-40 and the ensemble model mean underestimate the net SW radiation at TOA. For ERA-40 this can be (at least) partly explained by an overestimation of LWP in the region. Simulated subtropical trade wind cumulus has been reported to be too reflective in climate models compared to observations (e.g., Potter and Cess 2004; Karlsson et al. 2008). This might explain the ensemble model mean underestimation of net SW radiation in the Cu regions. In the ITCZ the ensemble model mean shows better agreement with CERES, while ERA-40 is associated with a negative TOA net SW radiation bias of ~50 W m^{-2}, most likely connected to the positive LWP and cloud cover bias in the region. Again, the variability between the different models is substantial and clearly problematic in particular in the context of coupled ocean–atmosphere seasonal and climate prediction.

5. Vertical cross sections

Figure 9 shows vertical cross sections of subsidence in Pa s^{-1} along the GPCI transect from the different models. Qualitatively all models produce (as expected) features that resemble the Hadley circulation with dominant upward motion over the ITCZ and a dominant subsidence region throughout the subtropical free troposphere.

In spite of the qualitative agreement, there are several substantial differences between the models. For example, some models, ETH/MPI being the most extreme case, exhibit a fairly shallow layer of upward vertical motion in the ITCZ (in the ETH–MPI model over the ITCZ the layer of upward mean vertical velocity does not appear to extend above 700 hPa). The width and strength of the deep convection regions are other examples of the differences between the models, with the GISS model having a fairly wide and weak deep convection (as given by the vertical velocity field) while ERA-40 has a relatively narrow and much stronger deep convection vertical velocity structure. Another relevant difference is the fact that some models have a peak of vertical velocity in the convective regions in the lower troposphere while others also have a peak in the upper troposphere.

In addition, and although the patterns are in general relatively similar between the different models, there are differences in the subsidence regions as well. In particular, the free-troposphere vertical structure of subsidence in the trade wind regions and the vertical extent of the subsidence field in the boundary layer can be quite different between the models. The vertical structure of subsidence is crucial in determining the vertical extent of boundary layer convection and the characteristics of clouds.

The corresponding results for relative humidity are shown in Fig. 10. Relative humidity is a particularly informative field in terms of the characterization of the atmospheric hydrologic cycle in a variety of aspects from boundary layer and cloud properties to the dryness of the subtropical free troposphere. As with subsidence, a first look at the different relative humidity model fields shows

that all models possess the qualitative characteristics of a Hadley-like circulation. The boundary layer evolves from shallow and cloudy (with high values of relative humidity) over the cold upwelling waters off California to a deeper trade-wind boundary layer over warmer waters. Over the warm regions of the ITCZ the troposphere is dominated by deep convection (in general, with high relative humidity values throughout the troposphere) and in the subtropical free troposphere the dynamics is dominated by the large-scale subsidence associated with very low values of relative humidity.

In spite of the qualitative agreement between the models, the level of disagreement is significant. In terms of the boundary layer the most obvious difference is related to how the boundary layer grows from the Sc regions to the Cu regions in the models. Some models show a low boundary layer height over the Sc regions [e.g., NCAR, UQM) often together with a low growth of the boundary layer over warmer waters, while other models seem to produce an excessive growth of the boundary layer reaching values that are not realistic (e.g., the DWD produces a boundary layer height over the trade cumulus regions close to 700 hPa). Note that we do not compare directly model relative humidity results with observations in this paper [e.g., results from comparisons with the Atmospheric Infrared Sounder (AIRS) are left for a future publication], and that this discussion is meant to highlight the differences between the models (and the ERA-40 analysis).

As discussed before concerning vertical velocity, models show substantial differences in terms of deep convection that are even more obvious when analyzing the vertical distribution of relative humidity along the GPCI transect. Differences are clear not only in terms of strength and width of deep convection but also in terms of wetness and dryness (in relative humidity terms) of particular regions of the atmosphere. For example, virtually all models have a minimum of relative humidity around 400 hPa but disagree on the absolute value of the relative humidity minimum. Some of the models (e.g., ETH–MPI, Météo-France, UCLA) have values of relative humidity that are lower than 20%, while other models (e.g., GFDL, JAMSTEC) have values close to 50%. Below the tropical tropopause the differences are also significant, with some models (e.g., GISS, CMC) showing values of relative humidity close to 40% while others [e.g., CSU multiscale modeling framework (MMF), ECMWF] have values close to 100%.

In the subsidence regions over the subtropical boundary layer, the models also show substantial differences highlighting the fact that the physics of the free troposphere in the models can be quite complex. Below the tropopause close to 35°N, models range from the very dry (e.g., DWD, GISS) with relative humidity close to 10% to the very wet with relative humidity close to 70% (e.g., CSU BUGS). All models exhibit a minimum value for relative humidity in some region of the subtropical free troposphere, but the location of this region can vary significantly from model to model. Some models exhibit this minimum above the stratocumulus regions (e.g., NCAR) while other models (e.g., GKSS), Meteo-France) exhibit a minimum much closer to the deep convection regions.

Figure 11 shows similar results for cloud fraction cross sections. This figure illustrates well the vast differences between models and is a good preamble for the detailed diagnostics and discussion that will follow in the subsequent sections. Qualitatively, virtually all models seem to follow the expected evolution of the boundary layer from the stratocumulus regions to deep tropics, but often with fairly significant differences. Some models [e.g., ECMWF, GFDL, UKMO) show a smooth and gradual evolution of the cloudy boundary layer height that, based on some previous studies, appears to be relatively realistic (e.g., Wyant et al. 1997; Wood and Bretherton 2004; von Engeln et al. 2005; Karlsson et al. 2010). But, there are many issues including (i) models that have stratocumulus clouds too close to the surface (e.g., NCAR); (ii) models that produce cloudy boundary layers that are too deep over the trades (e.g., DWD); (iii) models that produce a cloud evolution by generating two fairly distinct cloud layers (e.g., BMRC); (iv) models that produce very small values of cloud cover; and (v) models that show no clear evolution of the cloudy boundary layer from stratocumulus to cumulus (e.g., NCEP).

The fact that there are two sets of results from NCEP, coupled and uncoupled to an ocean model (NCEP GFG&MOM3 and NCEP, respectively), leads to some insight into the impact on clouds of the coupling to an ocean model. Both coupled and uncoupled versions show small amounts of boundary layer cloud fraction, with a peak positioned too far to the southwest and no clear evolution of the cloudy boundary layer from stratocumulus to cumulus. However, the uncoupled version produces larger values of cloud cover (close to 40%) than the coupled version (less than 20%), and the SST of the coupled model version is overestimated (Fig. 6). These results are associated with a well-known positive feedback between subtropical boundary layer clouds and the SST, where a negative bias in cloud cover and cloud water leads to warmer surface waters (due to increased shortwave radiation at the ocean surface) that, in turn, lead to even less clouds (e.g., Philander et al. 1996; Ma et al. 1996; Park et al. 2005; Teixeira et al. 2008). Interestingly, the coupled version produces more clouds in the upper tropospheric regions.

Over the ITCZ the differences in terms of cloud fraction are fairly large, with some models showing substantial

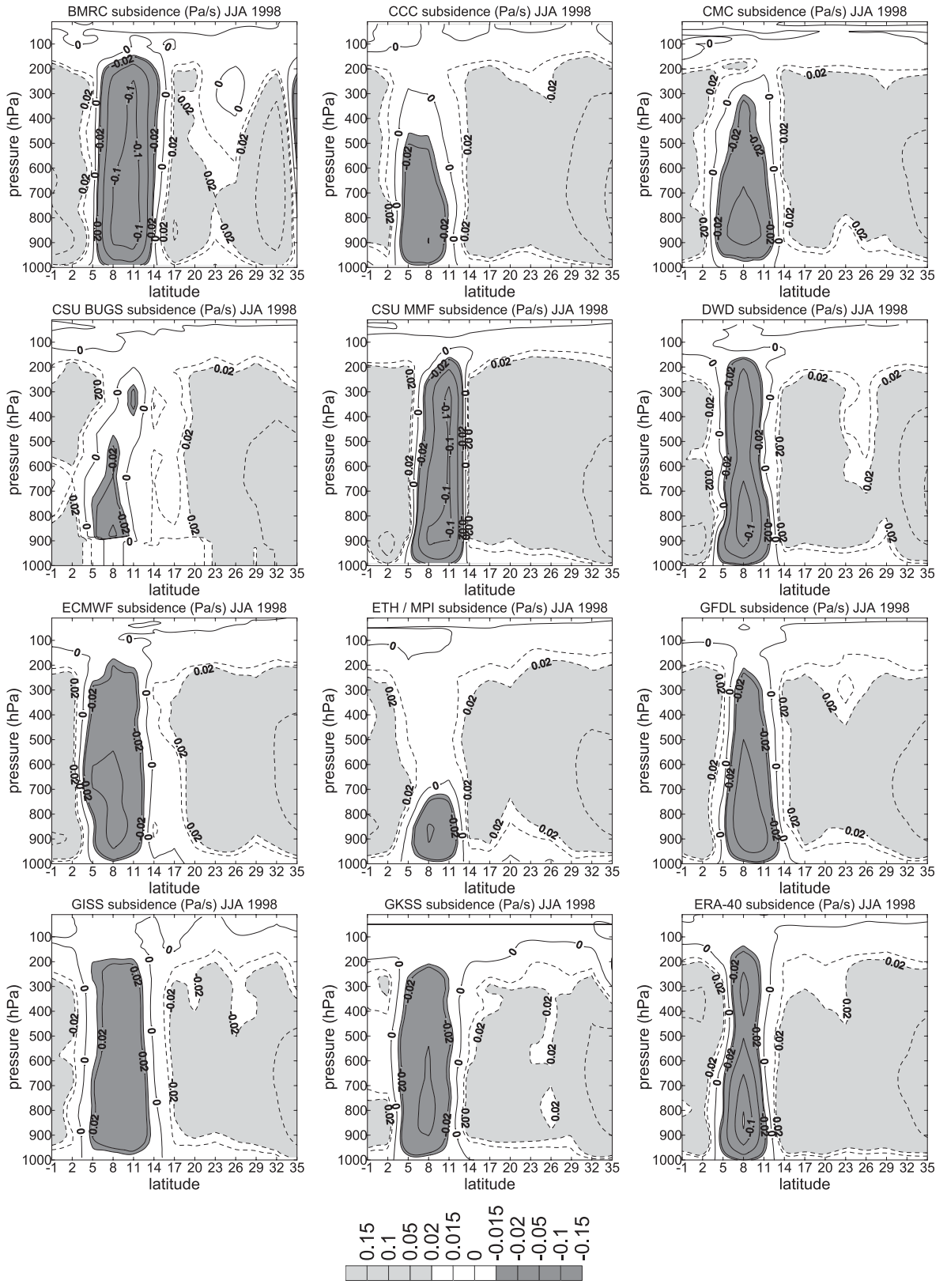

FIG. 9. Vertical cross sections of subsidence (Pa s^{-1}) along the GPCI transect for June–July–August 1998 from the different models and ERA-40 (shown twice for easier comparison).

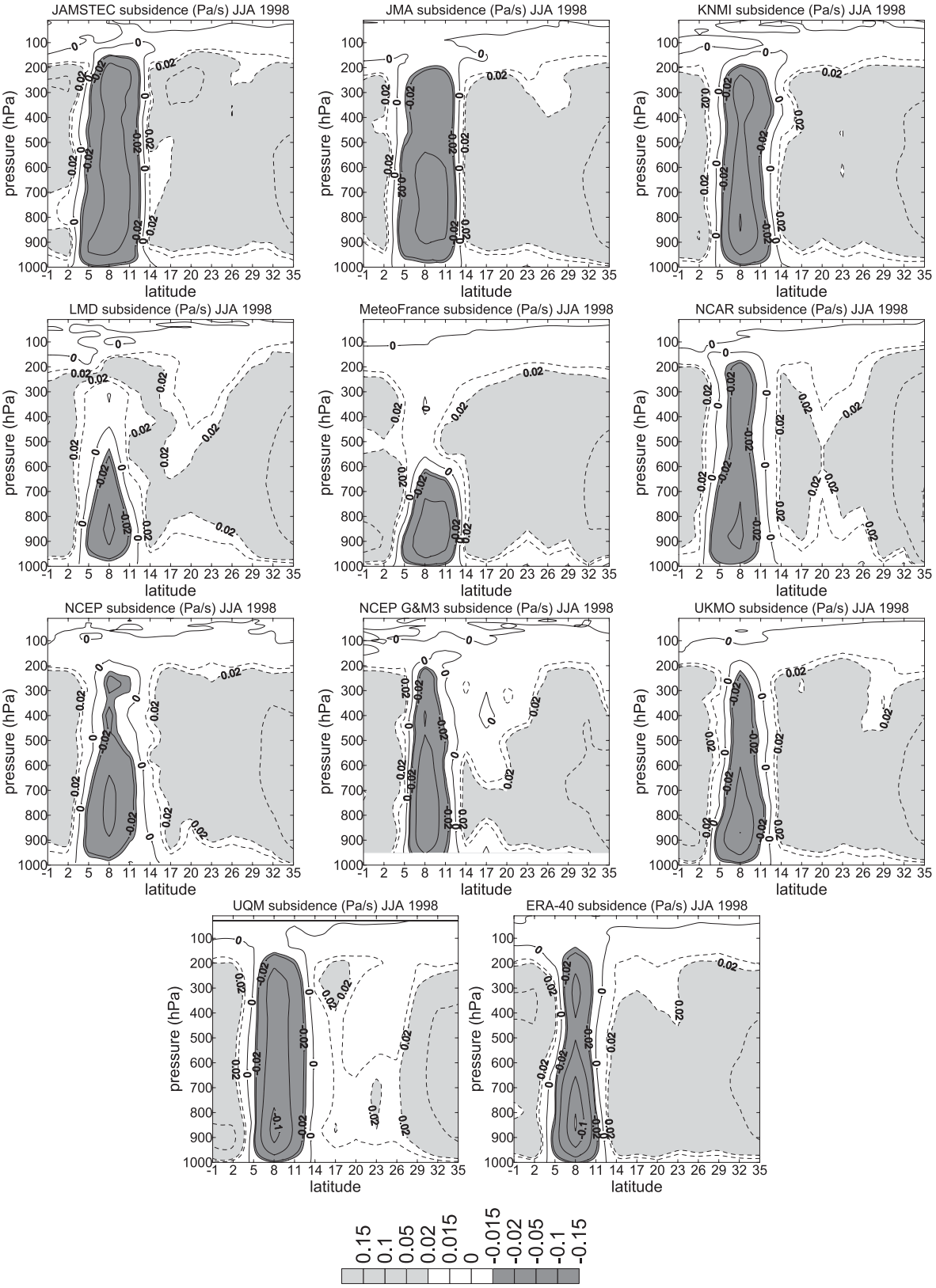

FIG. 9. (*Continued*)

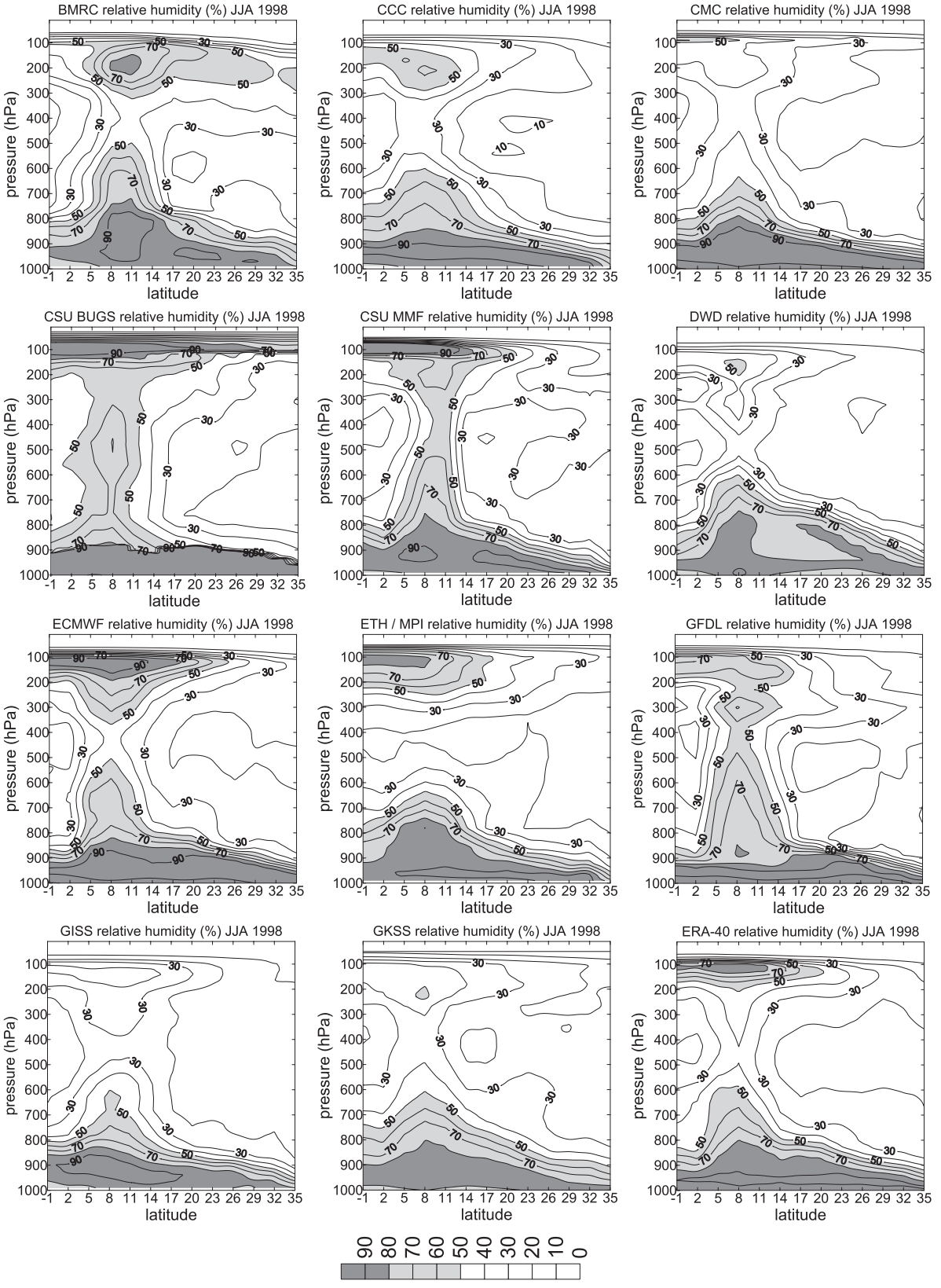

FIG. 10. Vertical cross sections of relative humidity (%) along the GPCI transect for June–July–August 1998 from the different models and ERA-40 (shown twice for easier comparison).

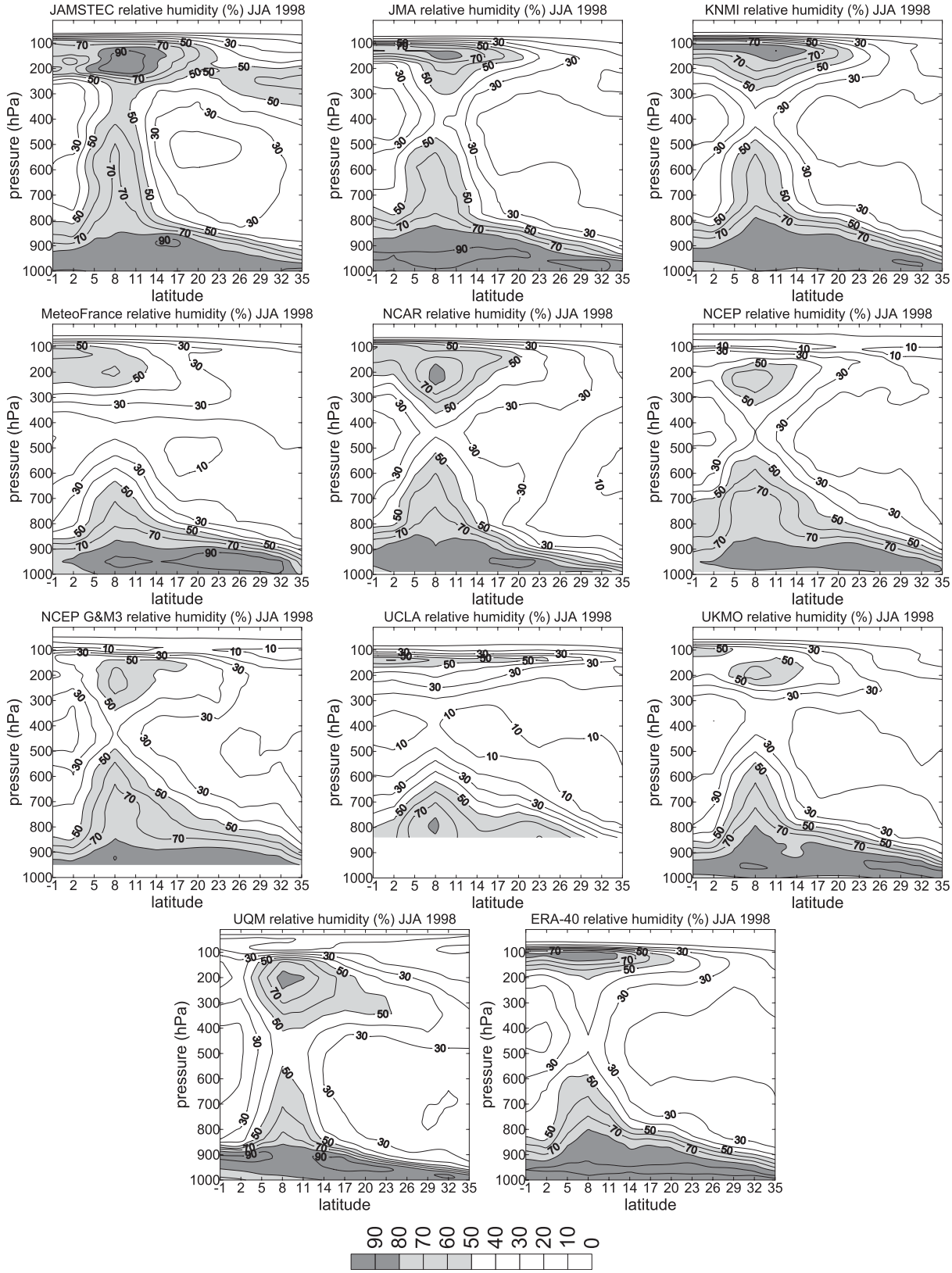

FIG. 10. (*Continued*)

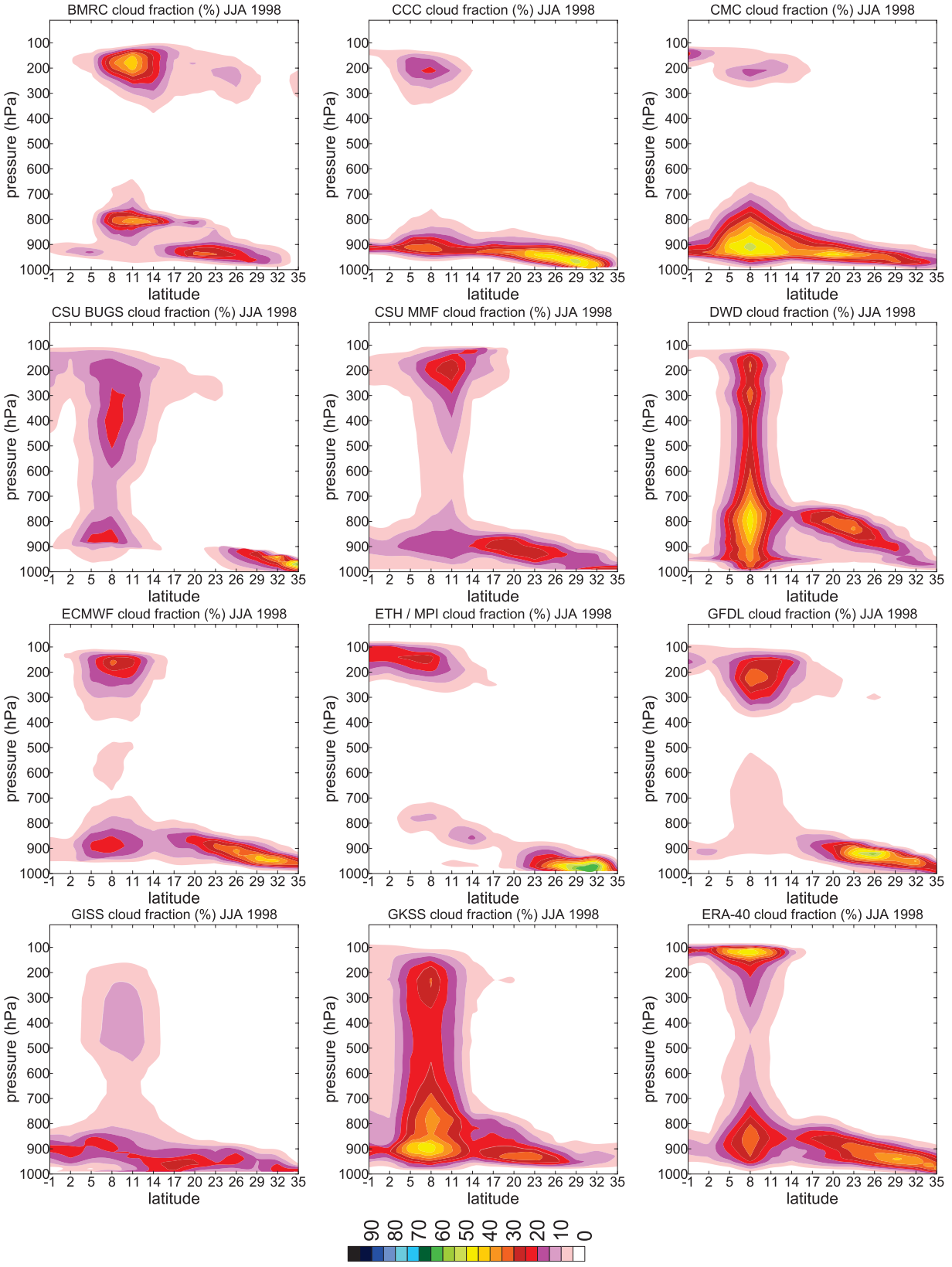

FIG. 11. As in Fig. 10, but of cloud fraction (%) at each level.

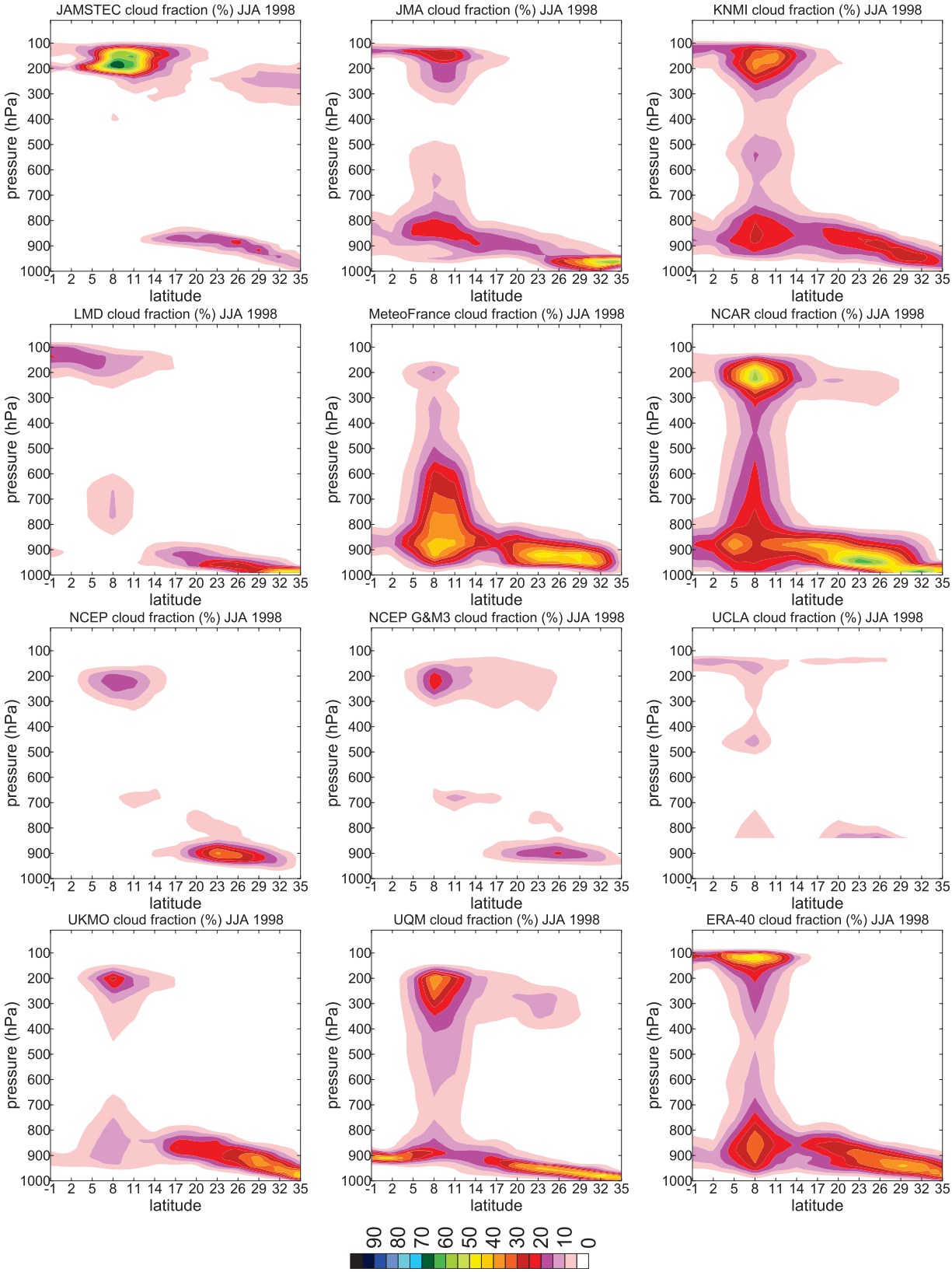

FIG. 11. (*Continued*)

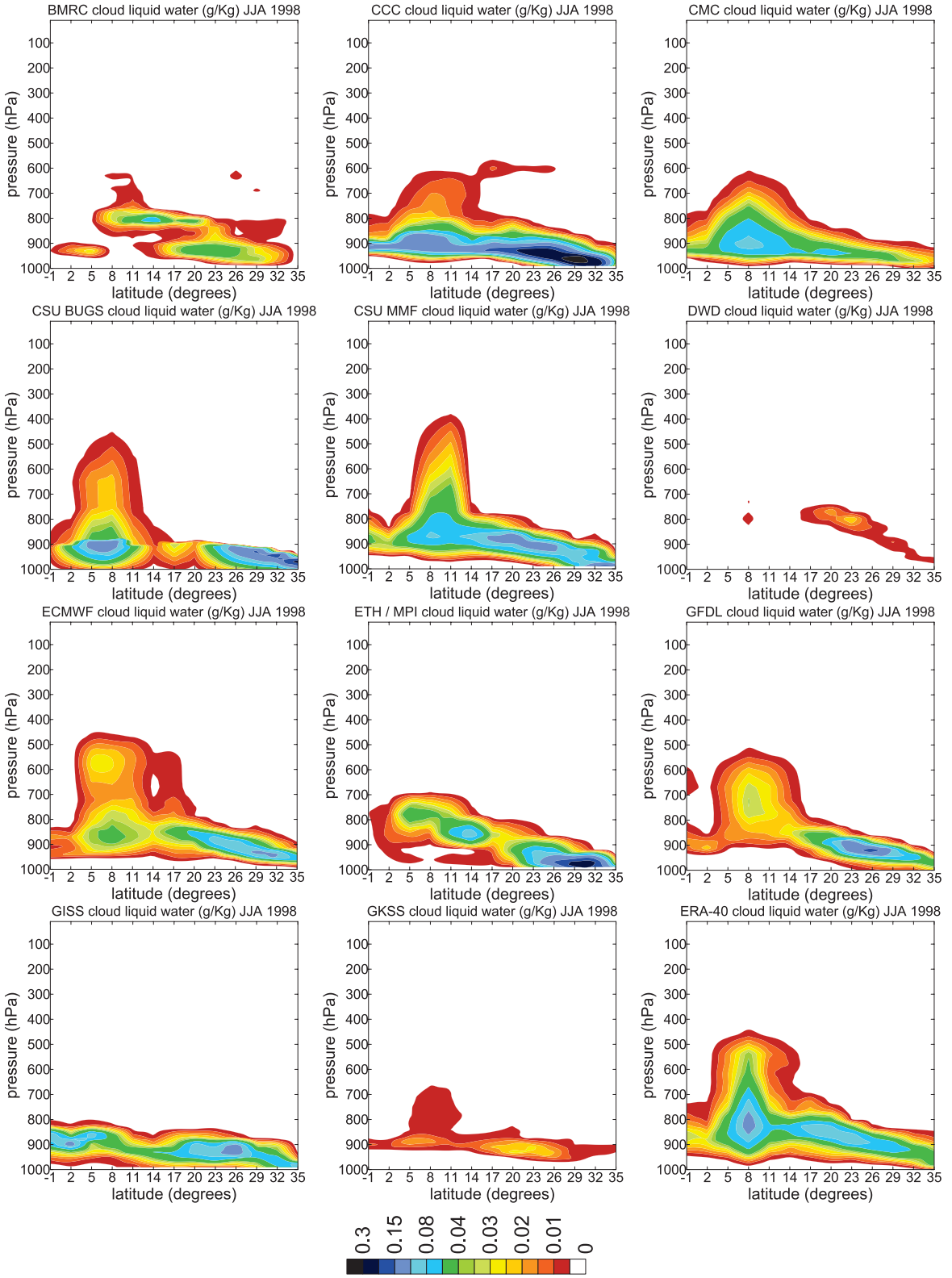

FIG. 12. As in Fig. 10, but of liquid water content (g kg^{-1}) at each level and with *CloudSat* observations.

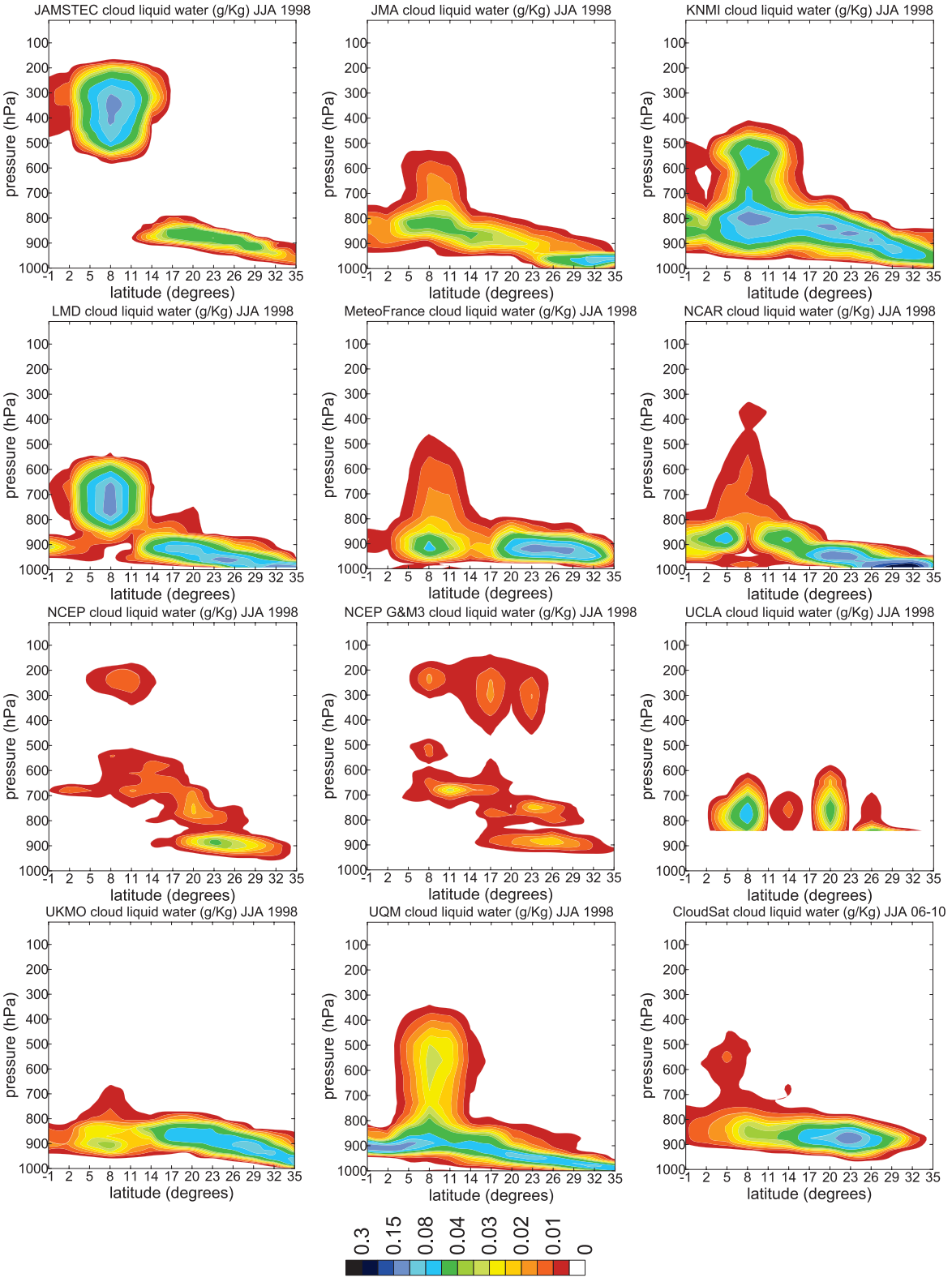

FIG. 12. (*Continued*)

amounts of cloud throughout the column (e.g., DWD, GKSS, NCAR) while others show negligible amounts in general (e.g., NCEP, UCLA). In the lower troposphere some models show large cloud amounts (e.g., Météo-France) while other models show virtually no clouds (e.g., JAMSTEC). In the upper troposphere some models have large values of cloud cover (e.g., NCAR) while others have relatively small values (e.g., GISS, Meteo-France).

Similar results for liquid water content are shown in Fig. 12, where in addition to the model data, the June–July–August climatology (2006–10) of liquid water content from *CloudSat* observations is plotted as well (e.g., Stephens et al. 2008). In most respects the liquid water content figures confirm the general results obtained for cloud fraction. However, there are some noteworthy features that are important to highlight. Some models erroneously produce liquid water at altitudes where most likely there is virtually no liquid water. At this stage it is unclear if these are postprocessing issues or real model problems.

Some models do reproduce the expected evolution of clouds along the transition from stratocumulus to cumulus with values of mean boundary layer liquid water that are roughly similar to the values obtained from *CloudSat*, which is clearly a positive sign both from a modeling and observational perspective. In this context it must be noted that *CloudSat* has some problems related to the retrieval of liquid water content in the boundary layer. Independent of specific issues related to the retrieval methodology, *CloudSat* has difficulties in obtaining reliable measurements close to the ground (roughly below 1 km above the surface) and its vertical resolution (~250–500 m) is not adequate to fully resolve the strong gradients close to the top of the boundary layer. Owing to these constraints, *CloudSat* is not able to produce a Sc-to-Cu transition as clearly as some of the models. In spite of this, *CloudSat* appears to support the idea that the cloudy boundary-layer height evolves from values close to 1 km above the surface near the coast of California to near 2 km in the trade cumulus regions.

Some of the models do exhibit what appears to be clearly pathological behavior in the subtropical boundary layer region—from models that show extremely low values of liquid water content (with maximum values close to 0.02 g kg^{-1}) to models that have different discrete layers of cloud in the vertical. In spite of the fairly poor model results (in general) in the Sc to Cu transition region, close to the ITCZ the model results can be considered even worse. In these deep tropical regions the model liquid water content vertical structure is almost as varied as the number of models. Hardly any two models seem to share a similar cloud liquid water vertical structure. If the *CloudSat* observations are used as guidance, it is possible to state that the UKMO appears as the model that is closest to the observations. But even this is arguable given the fairly ad-hoc manner in which the *CloudSat* retrieval algorithm discriminates between liquid water and ice (based on a simple mixed-phase relation using temperature from ECMWF analysis).

Overall, these figures illustrate the enormous difficulty that models have in even producing cloud vertical structures that are somewhat in qualitative agreement with each other and with the few global observations that exist.

Note that additional results and figures can be obtained at the GPCI/DIME webpage (see section 4).

6. Boundary layer cloud transition and statistics using sharp gradients

In the previous sections we reported on a variety of model diagnostics related to cloud regime transitions. This was done mainly with the goal of characterizing the mean thermodynamic structure in a variety of weather and climate prediction models. In this section, and in the following one, we use cloud data from the different models and from ISCCP observations to characterize in more detail the cloud transitions in the tropics and subtropics and to evaluate how well the models reproduce these transitions. In this context we try to relate the results of some of these models with the parameterizations used for representing clouds and the boundary layer.

In a previous section (Fig. 7b) the June–July–August 1998 mean TCC along the GPCI cross section for the model ensemble mean, ERA-40, and ISCCP is shown. This type of typical seasonal mean is calculated in a straightforward way, by estimating the temporal mean at each one of the cross-section points. However, since instantaneous (3-hourly) values of cloud cover can have sharp gradients along the GPCI transect, this averaging methodology will smooth out the gradients and will consequently lose information related to these discontinuities, which are important manifestations of the stratocumulus to cumulus transition.

In this section a different methodology to perform the averaging is proposed: by (i) determining the location of the first sharp gradient (specifically a drop with a particular threshold of 20 or 30%) in total cloud cover (TCC) along the transect starting at the northernmost point (Sc region) every three hours and then (ii) assuming uniform cloud cover to the northeast (NE) and southwest (SW) of the gradient's location by taking the spatial averages of TCC for all the points to each side (NE and SW) of the location of the sharp gradient. Figure 13 shows that, using this methodology, it is possible to capture some of the features of this discontinuous transition. The results in this figure correspond to TCC data from ISCCP and ERA-40. The left figure shows averaged TCC for both

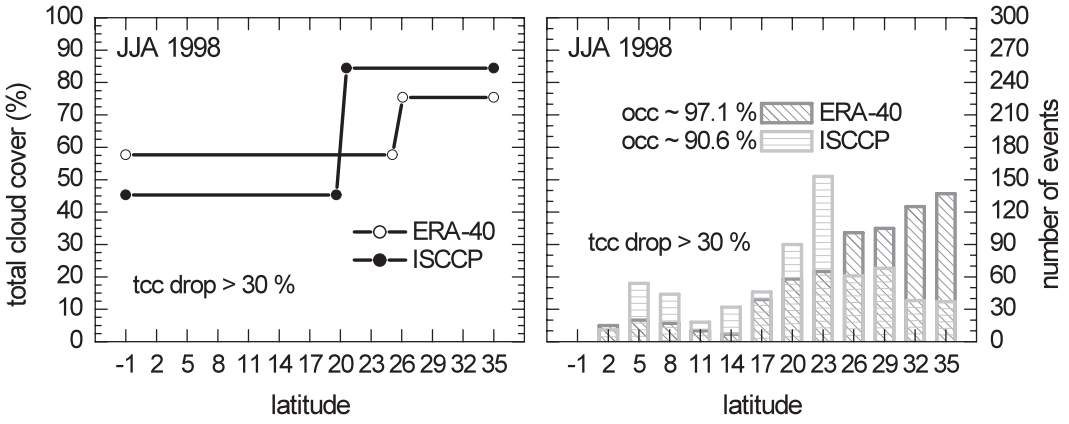

FIG. 13. Total cloud cover statistics for ISCCP and ERA-40 for June–July–August 1998 season along the GPCI transect using a methodology based on the identification of large gradients of TCC along the transect (see text for details): (left) averaged TCC for both ERA-40 and ISCCP based on this methodology and (right) histograms of the locations of these strong (>30%) gradients of TCC.

ERA-40 and ISCCP based on this methodology (i.e., averaged TCC for all the points south and north of each individual transition location) with the jump in TCC being located at the mean gradient location, while the figure on the right shows histograms of the locations of these strong (>30%) gradients of TCC. Using different thresholds for the drop of TCC (e.g., 20% or 30%) does not make much of a difference in the final mean results, which is a positive outcome regarding the robustness of the method. Note that even in the subtropics changes in TCC may not reflect only changes in boundary layer cloud cover [or low cloud cover (LCC)] but also changes in high and midlevel cloud cover.

There are substantial differences between ERA-40 and ISCCP in this context. The mean gradient strength is different between the two with values around 40% for ISCCP and 20% for ERA-40. The TCC values to the northeast and southwest of the gradient's location are quite different as well—to the northeast of the mean gradient location ISCCP TCC is about 10% larger than ERA-40 TCC, while to the southwest ERA-40 TCC is about 15% larger than ISCCP TCC. The mean location of the gradient is also different, with the ERA-40 location being at 26°N while the ISCCP location is at 20°N.

This analysis suggests that the ERA-40 negative cloud bias in the Sc regions is related, not only to the fact that TCC values in the Sc regions are in general lower than in the ISCCP data, but also to the fact that the transition from stratocumulus to cumulus (i.e., location of the mean gradient) is too far to the northeast—too early from a Lagrangian perspective—as compared to ISCCP observations.

An analysis of the histogram of locations of the sharp gradient for both ERA-40 and ISCCP (Fig. 13, right panel) clearly shows that the transition from stratocumulus to cumulus occurs too early (in a Lagrangian perspective) in the ERA-40 dataset with a histogram peak close to the coast of California (35°N), while the peak in the ISCCP observations is close to 23°N. Another difference between the two datasets is the occurrence (occ) of instantaneous gradients (larger than 30%) of TCC along the GPCI transect. It is slightly less in the ISCCP dataset (around 90% of the times) than in the ERA-40 dataset (around 97% of the times). Note that, for TCC gradients larger than 50%, ISCCP and ERA-40 have a frequency of occurrence greater than 60% and 70%, respectively (not shown).

Figure 14 shows similar results, but for the different models, where it is clear that there are substantial differences between the models in this context. These major differences exist in all of the main parameters being analyzed: the location and strength of the mean gradient, the cloud amount northeast and southwest of the mean gradient's location, and the characteristics of the histogram of the gradient locations.

In terms of the strength of the mean gradient there are important differences between models such as UCLA, CSU BUGS, and UKMO (with gradients stronger than 40% on the mean) and models such as CMC that have virtually no gradient in TCC between stratocumulus and cumulus regimes (recall that ISCCP has a value of around 40%). The stronger gradients in models such as UKMO and UCLA are probably related to the nature of the cloudy boundary-layer formulation. This will be discussed in more detail in the next section. In terms of the frequency of occurrence of gradients in TCC as large as 30%, most models are close to the results from ERA-40 with values just slightly below 100% except for the following models: NCAR, LMD, CCCma, and GISS, which have values below 90%.

Again, and as expected, there is a large amount of variability in terms of the TCC values to the northeast and southwest of the mean gradient locations for the different

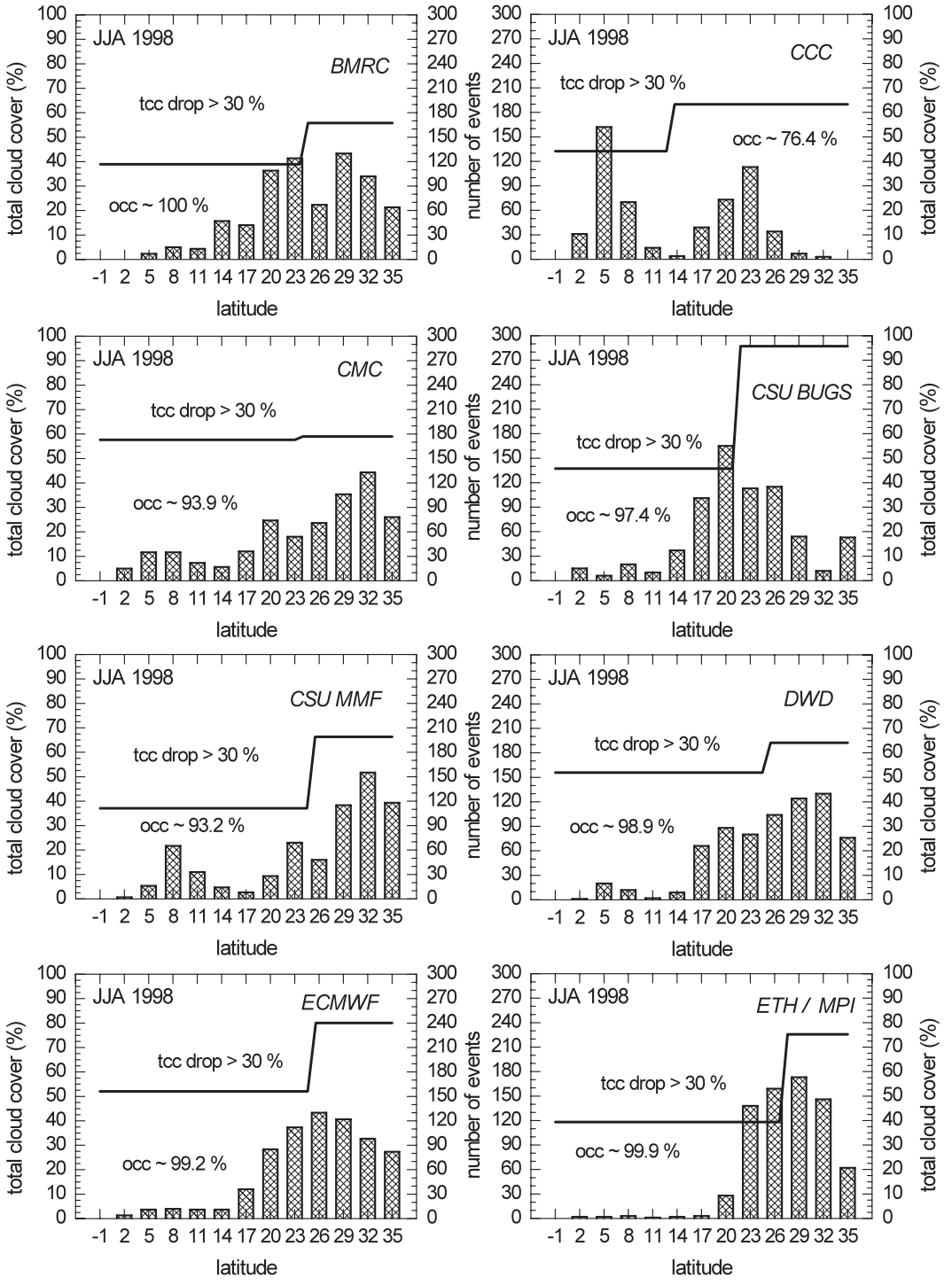

FIG. 14. Similar to Fig. 13, but for the different models.

models. In addition, there is a variety of shapes for the model histograms of the instantaneous locations of these strong gradients. Some models exhibit a one-peak distribution that can be well localized (e.g., UCLA) or have a large standard deviation (e.g., NCEP). Other models exhibit histograms with two prominent peaks (e.g., GFDL and CCC), while even more complex behaviors can be obtained (e.g., NCAR has three peaks with the most pronounced being at 5°N). Note that ISCCP exhibits two peaks: a dominant one at 23°N and a smaller one at 5°N.

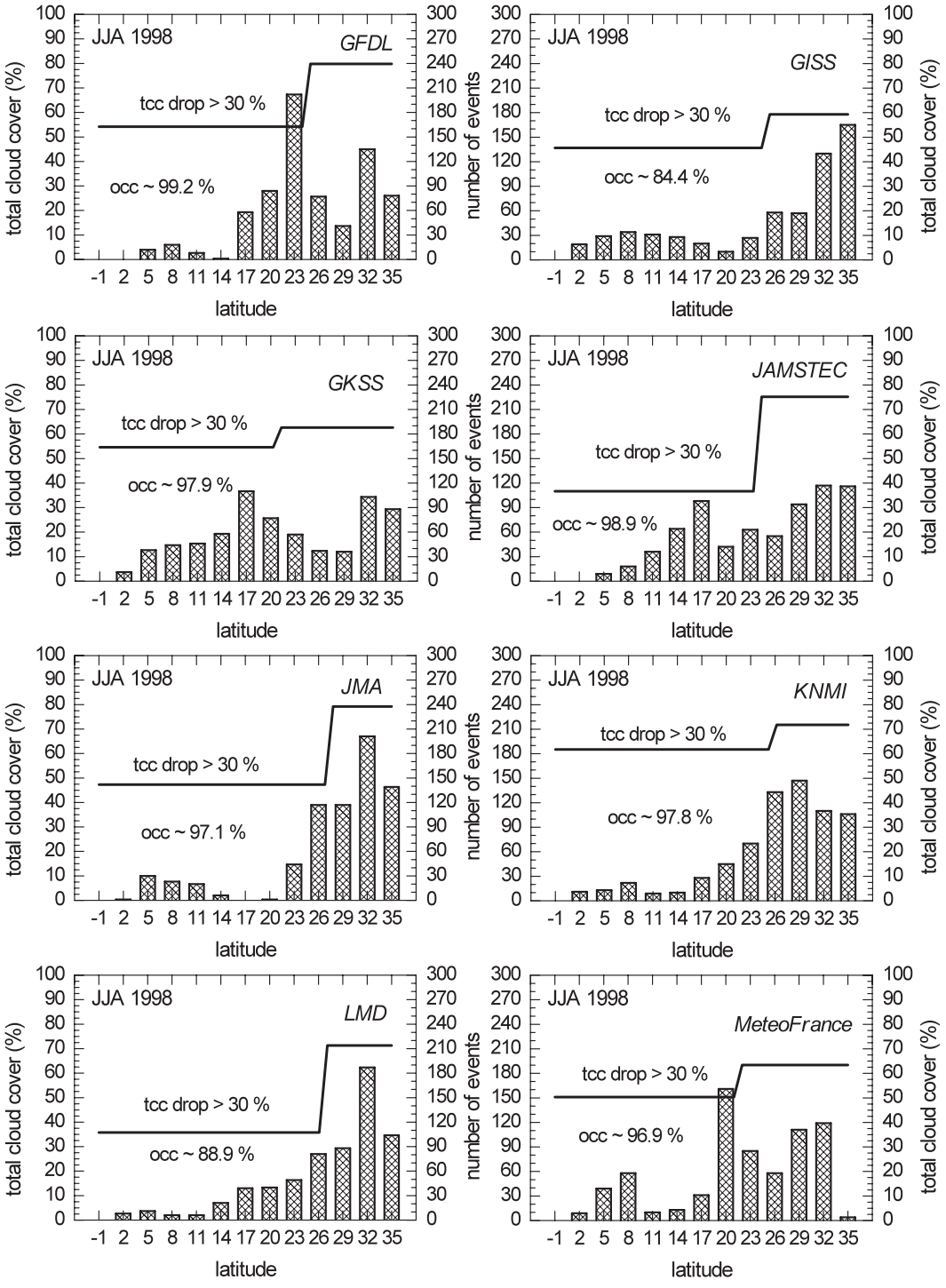

FIG. 14. (*Continued*)

7. Histograms of cloud cover transition

Diagnostics that analyze only seasonal mean values (e.g., mean cross section of TCC for example) are fairly incomplete in terms of providing information about the variability in time of a particular variable in a certain region (even the variance itself can be sometimes relatively meaningless for more complex distributions). Going back to the problem of how stratocumulus boundary layers transition to cumulus boundary layers along the trades,

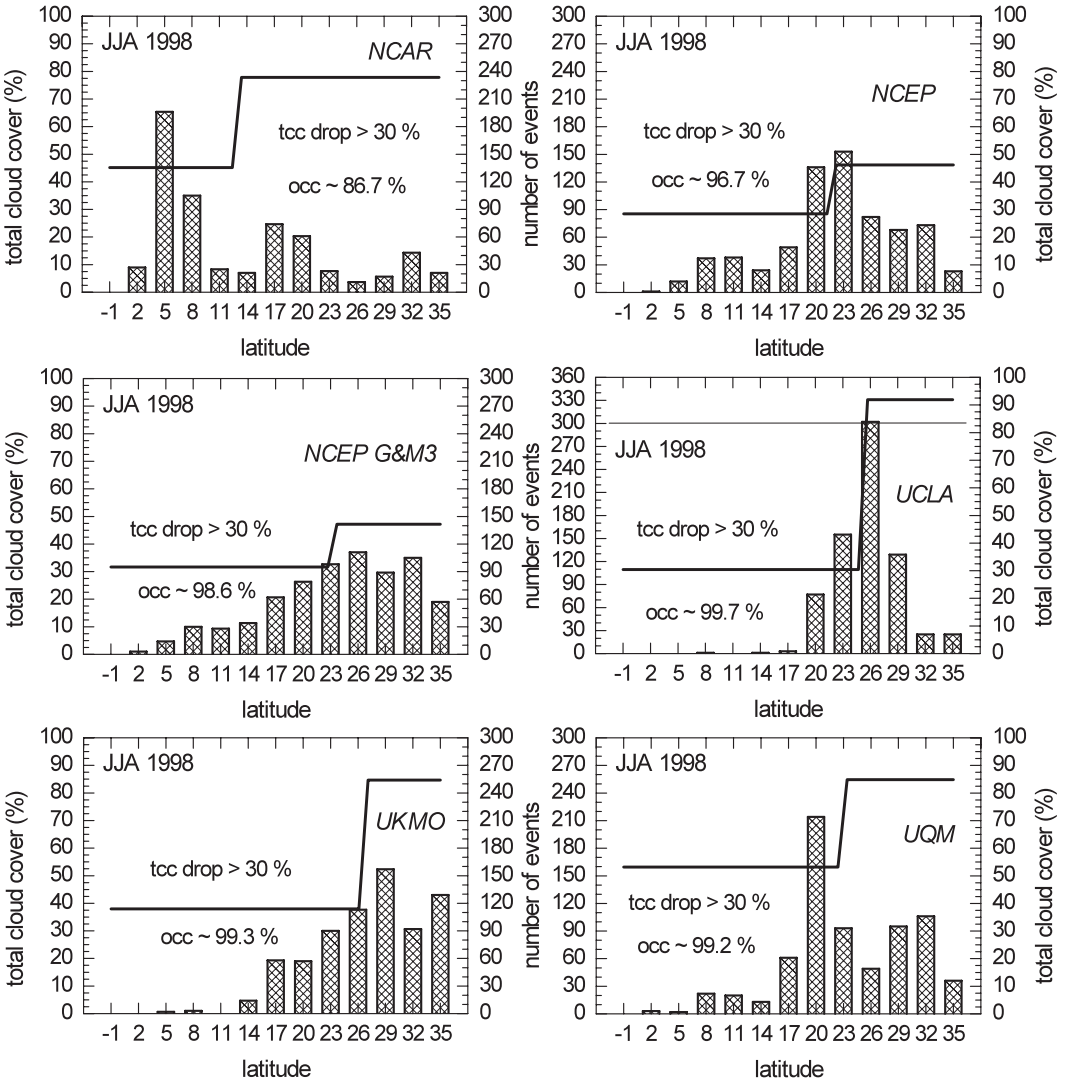

FIG. 14. (*Continued*)

valid questions regarding the model simulations are 1) how are the models reproducing this transition; 2) how do the models compare to satellite observations (e.g., ISCCP) of the transition; and 3) is this transition, in TCC, for example, fairly abrupt or pretty continuous in its nature?

As an attempt to answer these questions, Fig. 15 shows histograms of instantaneous TCC along the GPCI transect from the different models, ERA-40, and the ISCCP observations for JJA98. Again, a variety of behaviors between the different models is clear. In this context models such as NCAR and UKMO illustrate well two very distinct behaviors. It is clear that the differences in TCC between the models are more than just differences in terms of mean TCC, which is a traditional metric for the evaluation of cloud cover parameterizations in climate prediction models. In the UKMO model, the cloud cover shows a clear bimodal structure with most events occurring for TCC values either close to 0% or close to 100%. NCAR, on the other hand, shows a substantially distinct behavior with a relatively smooth transition from the subtropical stratocumulus regions to the tropics. These fairly distinct results were already clear when analyzing Fig. 5, which illustrated the differences between the GFDL and NCAR TCC in the GPCI point situated at 20°N. In practice, at latitudes close to 20°N, a typical transition region between stratocumulus and cumulus regimes, these three models (GFDL, UKMO, and NCAR) have fairly similar JJA98 mean TCC values. However, it is clear from these histograms that similar mean results can be associated with significantly different cloud distributions.

These two very distinct behaviors are associated with the manner in which clouds and cloud-related processes are

parameterized. In the NCAR model, cloud cover associated with the subtropical boundary layer is partly parameterized based on dependence on the lower-tropospheric stability (LTS) parameter, which is defined as the difference between the potential temperature at 700 hPa and at the surface (e.g., Klein and Hartmann 1993; Rasch and Kristjánsson 1998). This empirical relation is based on observations (e.g., Slingo 1980; Klein and Hartmann 1993) and versions based on similar ideas have been used as boundary-layer (stratocumulus) cloud cover parameterizations for some time (e.g., Slingo 1987). However, this empirical dependence is apparently valid in longer time scales (e.g., seasonal) but not necessarily at the typical time-step and horizontal gridbox scales (e.g., Kawai and Teixeira 2010). By utilizing this dependence between cloud cover and LTS directly as a cloud cover parameterization, the NCAR model is partly imposing a climatological value of cloud cover leading to the fairly continuous TCC transition shown in Fig. 15. Note however that, although the LTS parameterization is likely responsible for the behavior of the NCAR TCC statistics, this cannot be stated for sure because of a variety of reasons: total cloud cover is not the same as level-by-level cloud fraction (there is a cloud overlap calculation involved), the cloud fraction at each point and level is determined as some combination of different cloud fractions of which the LTS cloud fraction is only one, and it is also not clear how often the LTS cloud fraction parameterization determines the final values of cloud fraction.

The UKMO model (and partly GFDL) has a cloudy boundary layer parameterization based on the concept of ''distinct cloud regimes'' (e.g., Lock et al. 2000), which assumes that the subtropical boundary layer can be divided in a finite number of different types or regimes (e.g., stratocumulus, cumulus, transition from cumulus to stratocumulus). In this approach the problem of parameterizing boundary layer properties is apparently simplified by the fact that only a finite number of different physical regimes need to be represented. A key problem of this parameterization philosophy is the representation of the transitions between the different discreet regimes. This ''discrete'' nature of the UKMO cloudy boundary layer parameterization is presumably responsible for relatively sharp cloud regime transitions and consequently the bimodal nature of the TCC histograms.

In Fig. 15 ISCCP observations of TCC (shown twice at the bottom of each page) show results that are somewhere in-between these two extreme behaviors. Although ISCCP shows a certain degree of bimodality these results suggest that none of these more ''extreme'' parameterization philosophies produces a fully realistic answer when compared to the observations.

Although many of them do fall into one of these categories, models exhibit a variety of behaviors in terms of TCC histograms. The GISS model, for example, shows no apparent transition, while the CCC model exhibits quite a complex distribution. The UCLA model, on the other hand, shows a fairly random histogram. In addition, some models exhibit histogram peaks in specific regions that are not apparent in the observations: JAMSTEC has a clear 30% peak at 8°N, while KNMI has a 50% peak at around 23°N.

8. Low cloud cover versus vertical velocity and sea surface temperature

The period of this study (June–July–August 1998) is too short to obtain statistically significant results concerning relations between cloud properties such as cloud cover and other properties such as measures of vertical stability (e.g., Klein and Hartmann 1993; Wood and Bretherton 2006; Kawai and Teixeira 2010). However, it is still useful to investigate how different cloud structures produced by different models relate to meteorological quantities such as SST and subsidence along GPCI.

Previous studies have shown a significant relation between cloud cover and different variables that basically characterize atmospheric vertical stability in the cloudy boundary layer. Klein and Hartmann (1993) showed a strong relation between seasonal low cloud cover (averaged in fairly large regions of the oceanic subtropics) and lower tropospheric stability, while Wood and Bretherton (2006) showed improved dependencies using a variant of LTS. Kawai and Teixeira (2010) showed that not only cloud cover correlates better with a variable related to cloud top entrainment instability (CTEI), but that in addition higher moments of LWP (variance, skewness, and kurtosis) are also strongly related to this CTEI variable.

In the present study, the relation between low cloud cover (LCC), on the one hand, and vertical velocity and SST, on the other, in a few models and ERA-40, is investigated in more detail. Both vertical velocity and SST are known to be related to LCC in the subtropics. Over the Sc regions, with cold SSTs and large values of subsidence, LCC values are typically large. While being advected over warmer waters and regions with lower values of subsidence, LCC typically decreases.

The 2D joint histograms of SST and subsidence at 700 hPa for the period JJA98 are analyzed (not shown) for ERA-40 and the following models: NCAR, GFDL, UKMO, and the NCEP coupled simulation. The three uncoupled models show a similar behavior with larger values of subsidence clearly associated with the coldest temperatures, and for SSTs generally above 292 K the mean subsidence (for each SST) is fairly constant and just

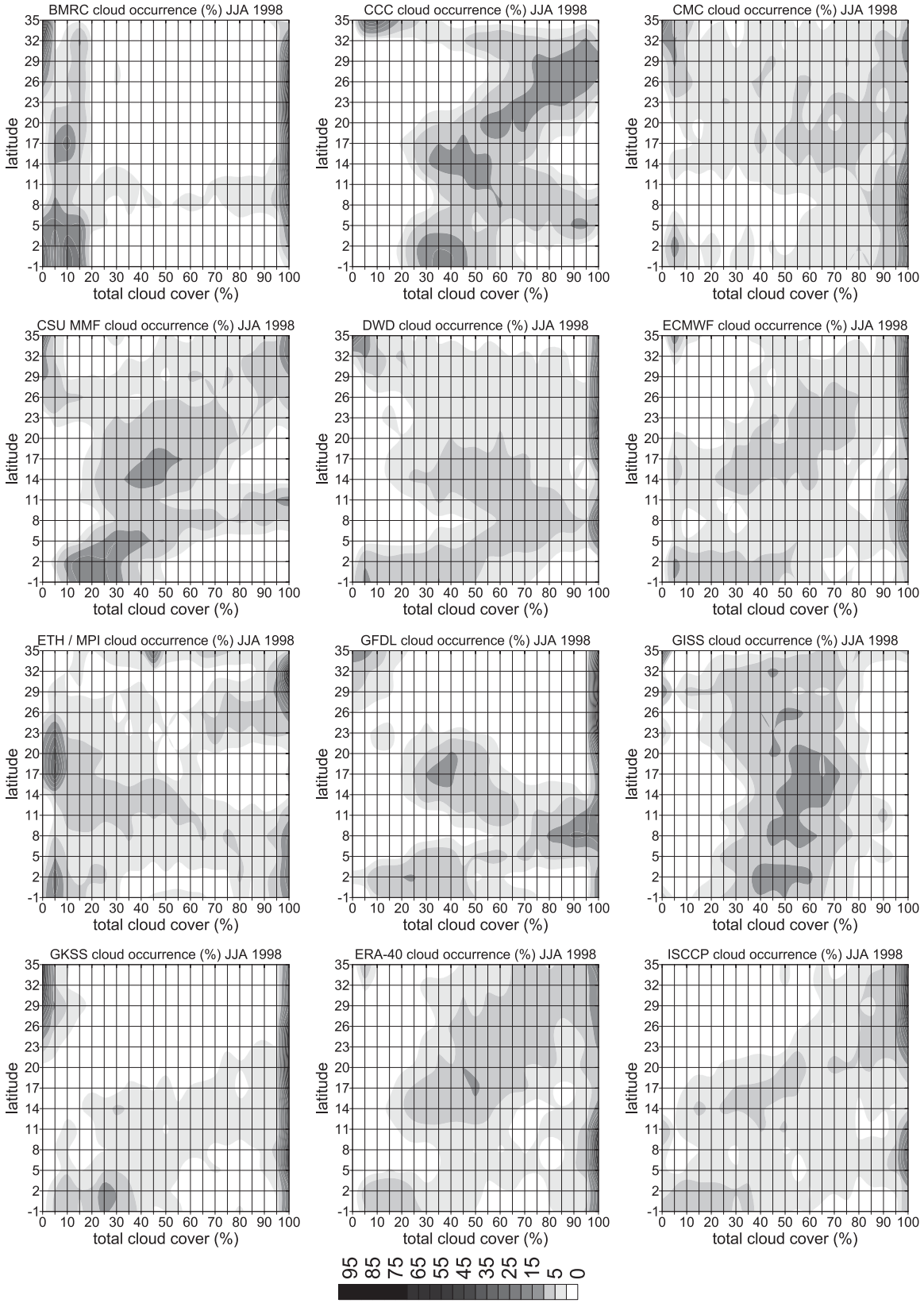

FIG. 15. Histograms of total cloud cover along the GPCI transect for the models, ERA-40 and ISCCP.

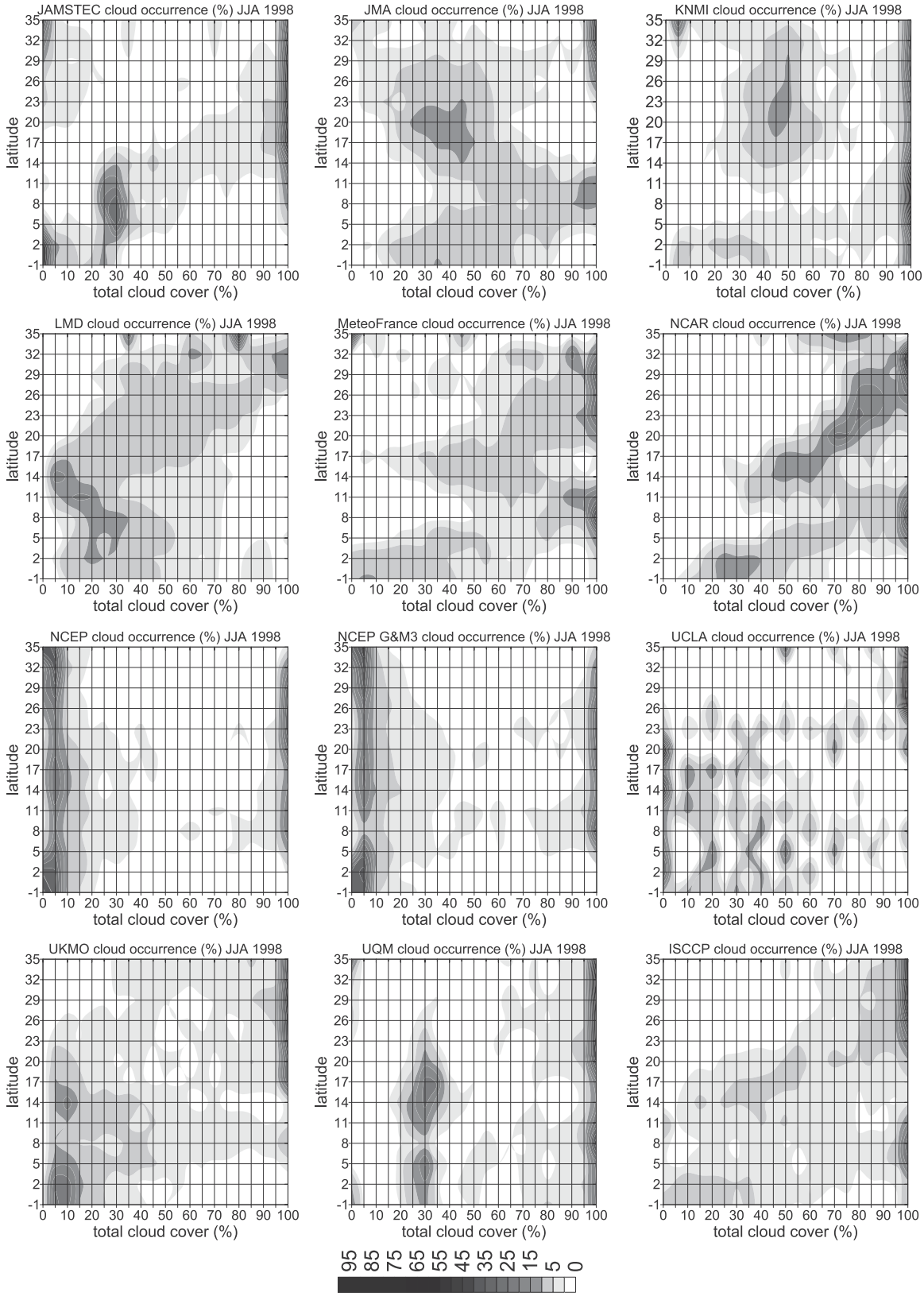

FIG. 15. (*Continued*)

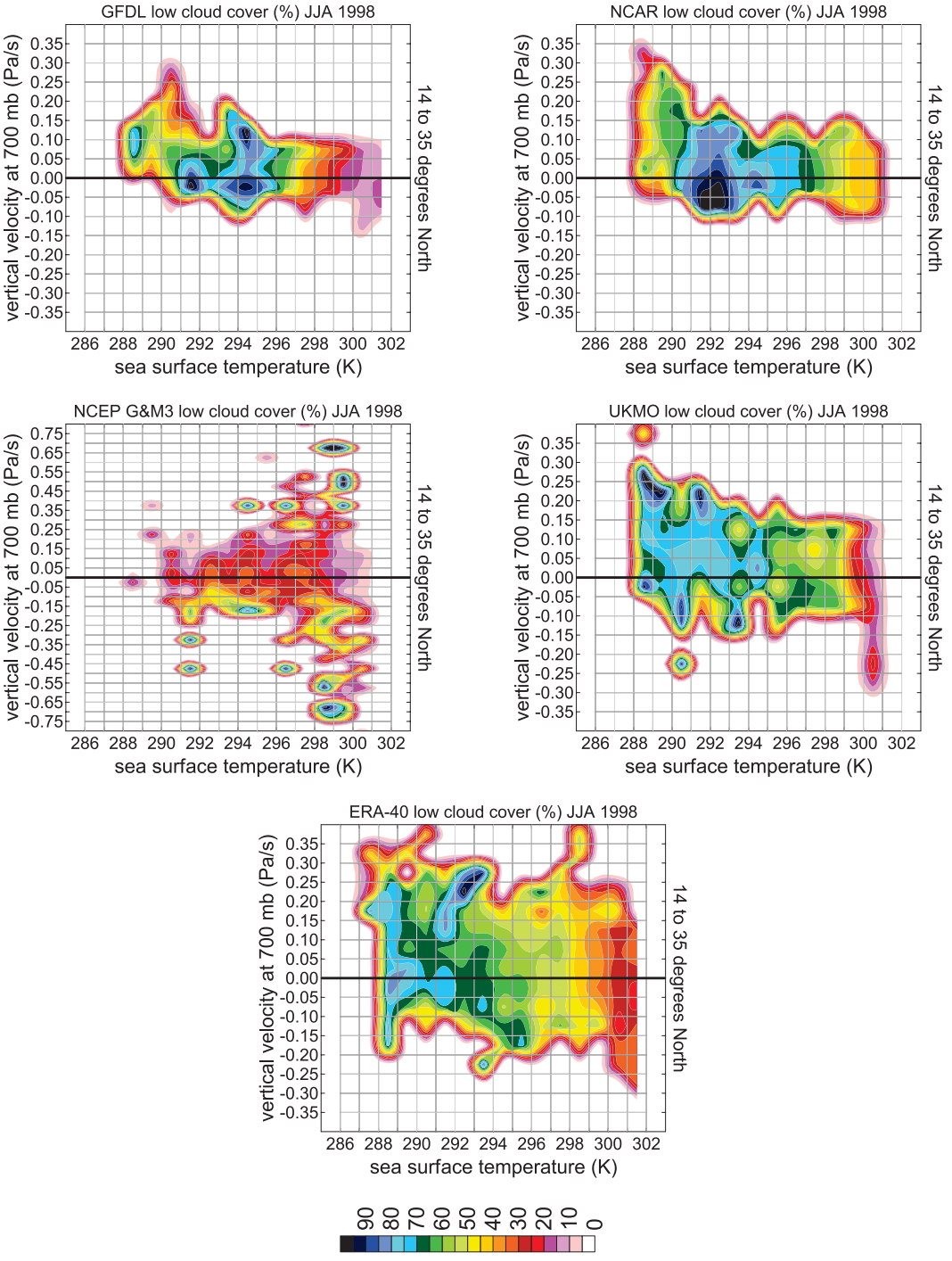

FIG. 16. Low cloud cover as a function of SST and subsidence (pressure vertical velocity) along GPCI for JJA98 for four models and ERA-40. Note the different vertical axis limits for the NCEP coupled simulation.

above zero. NCAR does show larger values of subsidence in the coldest regions, which may be associated with the low altitude of its boundary layer clouds close to the coast. Although different in the details, ERA-40 resembles these three models, while the NCEP coupled simulation is clearly different. As expected due to its positive SST biases, the NCEP coupled simulation does miss the coldest SSTs.

Figure 16 shows results for LCC (in percent) as a function of SST and subsidence at 700 hPa for the four

models discussed above and ERA-40. A clean and clear relation among LCC, SST, and subsidence is not obvious from these plots, although it is apparent that larger values of LCC are associated with lower values of SST. It is also clear that, while in the UKMO and ERA-40 there is a gradual LCC transition as a function of SST, NCAR and GFDL show LCC peaks that are not associated with the coldest temperatures and are related to negative subsidence values. In addition, except maybe for ERA-40 and the UKMO model, it is fairly difficult to argue that, from these figures, there is any type of relation between LCC and subsidence. The NCEP coupled simulation results appear fairly random, with large values of LCC associated with both large positive and negative values of subsidence (although these events are rare).

9. Conclusions

In this paper an analysis of cloud transitions, in weather and climate prediction models, in tropical and subtropical regions is performed. Three-hourly datasets from a variety of models were used in the context of the GCSS/WGNE Pacific Cross-section Intercomparison (GPCI) for the June–July–August 1998 season. The focus is on studying cloud cover changes from extensive stratocumuli decks (with high values of cloud cover) to situations where cumuli (with low values of cloud cover) dominate. This is an important transition in the context of cloud–climate feedbacks, and characterizing how different models simulate this transition is a key task in model diagnostics.

This study reiterates many of the general concerns in terms of simulations of clouds and cloud-related processes (which apply not only to models but also to reanalysis such as ERA-40), some of them already reported in the EUROCS (Siebesma et al. 2004) and other similar diagnostic studies. Models tend to underestimate clouds in the stratocumulus regions, both in cloud cover (as compared to ISCCP) and liquid water path (as compared to SSM/I), which is reflected in positive shortwave radiation biases at the surface and top of the atmosphere. In the deep tropics, ERA-40 (in particular) overestimates cloud cover, liquid water path, precipitation and (as a consequence) underestimates the outgoing longwave radiation.

A major concern is the large spread in the results between the different models in terms of cloud cover, liquid water path, and shortwave radiation. Although all models exhibit a Hadley-like circulation (in terms of vertical velocity and relative humidity) the differences between them are substantial, in particular, in terms of cloud cover and liquid water content vertical structure. The fact that for cloud-related variables ERA-40 often produces results that are less realistic than many of the models is a great illustration of the problems associated with assimilating cloud-related information in weather prediction models.

It is important that the models should be able not only to produce realistic values of mean cloud cover over the stratocumulus and cumulus regions (which has been historically a major problem for climate and weather prediction models) but also be able to capture some of the more dynamic features that are discussed in this paper such as the sharp gradients of cloud cover along the GPCI cross section and cloud cover histograms in general.

An analysis of the results using these tailored diagnostics allows one to dig deeper into the reasons for the deficiencies exhibited by the models and to connect these shortcomings with parameterization methodologies. Comparing the cloud cover mean statistics obtained by taking into account sharp gradients in cloud cover along the GPCI transect, allows one, for example, to determine that the negative cloud bias of ERA-40 in the stratocumulus regions (as compared to ISCCP) is associated (i) not only to lower values of cloud cover in these regimes but also (ii) to a stratocumulus-to-cumulus transition that occurs too early along the trade-wind Lagrangian trajectory (too much to the northeast).

It is shown that histograms of cloud cover along the GPCI cross section differ significantly from model to model. In particular, some models (e.g., UKMO) exhibit a quasi-bimodal structure with cloud cover being either close to 100% or close to 0%, while other models (e.g., NCAR) show a more continuous transition. The ISCCP observations show results that are somewhere in-between these two extreme behaviors. We speculate that these different patterns reflect the different nature of the cloud and boundary layer parameterizations, with some models (e.g., UKMO) basing their parameterizations on the idea of distinct regimes (with the consequent sharp transitions between them) while other models base their parameterizations on ''climatological'' relations (e.g., NCAR).

Acknowledgments. We acknowledge the crucial feedback received from a variety of participants in the workshops and conferences where results of this study have been presented and discussed. JT and SC acknowledge the support of the NASA MAP program and the Office of Naval Research. Part of the research described in this publication was carried out at the Jet Propulsion Laboratory, California Institute of Technology, under a contract with the National Aeronautics and Space Administration. We acknowledge the important feedback from the four anonymous referees.

TABLE A1. Basic information about the models that were used for the GPCI simulations analyzed in this work. This table lists the organization responsible for the model, the model name and type, the horizontal and vertical resolutions used in the simulations, and the model references (a list of the acronyms and abbreviations present in this table can be found in Table A2 below).

Model information					
Organization	Model*	Type	Horizontal resolution	Vertical levels	Model reference
BMRC (Aus)	BAM 4.0.21	Global	T63	60	Zhong et al. (2001)
CCC (Can)	CCCma	Global	T47	35	von Salzen et al. (2005)
CMC (Can)	GEM	Regional	0.5° × 0.5°	53	Côté et al. (1998)
CSU (US)	BUGS	Global	2.5° × 2.5°	29	Colorado State University (2010)
CSU (US)	MMF	Global/MMF	T42	30	Khairoutdinov et al. (2005)
DWD (Ger)	GME	Global	59.9 km	31	Majewski et al. (2002)
ECMWF (UK)	ECMWF	Global	T399	62	ECMWF (2006)
ETH–MPI (Ger)	ECHAM5	Global	T42	19	Roeckner et al. (2003)
GFDL (US)	AM2p12b)	Global	2.0° × 2.5 °	24	Anderson et al. (2004)
GKSS (Ger)	CLM	Regional	50 km	32	Steppeler et al. (2003)
JAMSTEC (Jap)	AFES2)	Global	T239	96	Kuwano-Yoshida et al. (2010)
JMA (Jap)	GSM0412	Global	T106	40	Matsumura et al. (2002)
KNMI (Ned)	RACMO2.1	Regional	0.5° × 0.5°	40	van Meijgaard et al. (2008)
LMD (Fra)	LMDZ4	Global	2.50° × 3.75°	19	Hourdin et al. (2006)
Météo-France (Fra)	ARPEGE	Global	T63	31	Gibelin et al. (2003)
NASA–GISS (US)	GISS III 3.3	Global	2.0° × 2.5°	32	Schmidt et al. (2006)
NCAR (US)	CAM3.0	Global	T42	26	Collins et al. (2006)
NCEP (US)	GFS&MOM3	Global coupl.	T382	64	Saha et al. (2006)
NCEP (US)	GFS	Global	0.5° × 0.5°	64	Environmental Modeling Center (2003)
UCLA (US)	UCLAtm7.3	Global	2.5° × 2.0°	29	Gu et al. (2003)
UCSD (US)	RSM	Regional	180 km	17	Juang et al. (1997)
UKMO (UK)	HadGAM	Global	1.250° × 1.875°	38	Johns et al. (2004)
UQM (Can)	CRCM	Regional	180 km	29	Plummer et al. (2006)

* Partial list of full model names: BAM 4.0.21 (Bureau of Meteorology unified atmospheric model version 4.0.21), GEM (Global Environment Multiscale), GME (Global Model Europe), M2p12b (Atmospheric Model 2p12b), AFES2 (Atmospheric GCM for the Earth Simulator version 2), GSM0412 (Global Spectral Model), RACMO2.1 (Regional atmospheric climate model version 2.1), CAM3.0 (Community Atmosphere Model, version 3.0), GFS (Global Forecast System) and MOM3 (Modular Ocean Model, version 3), RSM (Regional Spectral Model), HadGAM (Hadley Centre Global Atmosphere Model), and CRCM (Canadian Regional Climate Model).

APPENDIX A

Description of the Models that Participated in the GPCI Study

A brief description of the models used in this study is listed in Table A1 (model acronyms and abbreviations are listed in Table A2).

APPENDIX B

GPCI Project Protocol

GPCI can be seen as a level-2 model intercomparison project (Gates 1992) in which all of the participating models have to follow the same line of predefined project specifications and protocols: i) simulations made under standard conditions, ii) common diagnostics in standard format, and iii) validation against common data.

Though standardized, the specifications were kept at a relatively generic level with the basic condition being that the models should run in climate mode (i.e., without data assimilation) and using prescribed SSTs as a boundary condition. As the periods of interest were the seasons June–July–August 1998 and 2003, the simulations started 20 May 1998 and 2003. The requested GPCI output corresponds to the periods between 1 June and 31 August 1998 and 2003.

Regarding the geographical area of interest, it was requested that model data should be sent for i) 13 locations along the GPCI cross section starting at 35°N, 125°W and proceeding southwestward at 4° longitude and 3° latitude steps to 1°S, 173°W and ii) locations every 5° × 5° in a grid ranging from −5° to 45°N, 160° to 240°E (referred to as the 2D maps).

Finally, the simulation results were submitted in high temporal resolution every 3 h at hours 00, 03, 06, 09, 12, 1500, 18, and 21 (UTC) and at full vertical resolution, that is, on model levels. Note that not all variables were available from all of the models.

TABLE A2. Acronyms and abbreviations for Table A1.

Aus	Australia
BMRC	Bureau of Meteorology Research Centre
Can	Canada
CCC	Canadian Centre for Climate modeling and analysis
CMC	Canadian Meteorological Centre
CSU	Colorado State University
DWD	Deutsche WetterDienst
ECMWF	European Center for Medium-Range Weather Forecasts
ETH	Eidgenössische Technische Hochschule
Fra	France
Ger	Germany
GFDL	Geophysical Fluid Dynamics Laboratory
GISS	Goddard Institute for Space Studies
GKSS	Gesellschaft für Kernenergieverwertung in Schiffbau und Schiffahrt
JAMSTEC	Japan Agency for Marine-Earth Science and Technology
Jap	Japan
JMA	Japan Meteorological Agency
KNMI	Koninklijk Nederlands Meteorologisch Instituut
LMD	Laboratoire de Météorologie Dynamique
MPI	Max Planck Institute for Meteorology
NASA	National Aeronautics and Space Administration
NCAR	National Center for Atmospheric Research
NCEP	National Centers for Environmental Prediction
Ned	The Netherlands
UCLA	University of California Los Angeles
UCSD	University of California San Diego
UK	United Kingdom
UKMO	UK Meteorological Office
UQM	University of Quebec at Montreal
US	United States of America

APPENDIX C

Observational Data Used in the GPCI Study

The bulk of the observational data used in this study, described in Table C1 (see [Table C2 for acronyms and abbreviations), was retrieved from the GCSS-DIME Web site in formats prepared for the GPCI project area of interest: see "CROSS-PAC" and "GPCI" at http://gcss-dime.giss.nasa.gov/. CERES ES9 data were obtained from the Atmospheric Science Data Center at the NASA Langley Research Center (http://eosweb.larc.nasa.gov/).

The SSM/I data and images are produced by Remote Sensing Systems (RSS) and sponsored by the NASA Pathfinder Program for early Earth Observing System (EOS) products. SSM/I is onboard polar orbiting satellites, property of the Defense Meteorological Satellite Program (DMSP). Retrievals from three DMSP satellites carrying SSM/I (F11, F13, and F14) operational during June–July–August 1998 were used in this study. RSS SSM/I can be found online at http://www.remss.com/ssmi/ssmi_description.html.

The GPCP dataset combines precipitation information from several sources. Microwave estimates are based on SSM/I, infrared (IR) precipitation estimates are obtained from geostationary satellites and polar-orbiting satellites, and gauge data are assembled and analyzed by the Global Precipitation Climatology Centre (GPCC).

A hierarchy of geostationary [GOES, geosynchronous meteorological satellite (GMS), Meteosat] and polar orbiting (NOAA) satellites are used by ISCCP to retrieve and calculate cloud related products (ISCCP at NASA GISS available online at http://isccp.giss.nasa.gov/products/onlineData.html).

A note on the treatment of ISCCP total cloud cover data

For the total cloud cover calculated from the cloud-top pressure and cloud optical thickness (PCTAU) dataset, the IR-only nighttime results for every 3-hourly retrieval were adjusted by adding the daytime difference between VIS/IR and IR-only, linearly interpolated between the dusk and dawn values (a similar procedure was applied to the retrieved DX data).

TABLE C1. Basic information on the observational datasets that were used for the evaluation of the GPCI simulations analyzed in this work. This table lists the data center source of the observations, the dataset name, the horizontal and temporal resolutions of the data products, and the parameters retrieved (a list of the acronyms and abbreviations present in this table can be found in Table C2 below).

Observational Datasets					
Source	Dataset	Reference	Hor. res.	Δt	Parameter
ASDC	CERES ES9	Wielicki et al. (1995)	2.5° × 2.5°	Monthly	SWFTOA, OLR
GCSS-DIME	SSM/I	Wentz (1997)	0.25° × 0.25°	2-daily	TWV, LWP
GCSS-DIME	ISCCP DX	Rossow and Schiffer (1999)	0.5° × 0.5°	3-hourly	TCC
GCSS-DIME	ISCCP PCTAU (D1)	Rossow and Schiffer (1999)	GPCI cross section	3-hourly	TCC
GCSS-DIME	GPCP v.2	Huffman et al. (1997)	1° × 1°	Daily	Precipitation
CloudSat	CWC RO4	Li et al. (2008)	1° × 1°	Daily	LWC

TABLE C2. Acronyms and abbreviations for Table C1 datasets and parameters.

ASDC	Atmospheric Science Data Center
CERES	Clouds and the Earth's Radiant Energy System
DIME	Data Integration for Model Evaluation
ES9	ERBE-like Science product 9
GCSS	GEWEX Cloud System Study
GPCP	Global Precipitation Climatology Project
LWP	Liquid water path
NASA	National Aeronautics and Space Administration
SW TOA	Net shortwave radiation at the top of the atmosphere
OLR	Outgoing longwave radiation
Precip	Precipitation
PCTAU	Cloud-top pressure (PC) and cloud optical thickness (TAU)
SSM/I	Special Sensor Microwave Imager
TCC	Total cloud cover
TWV	Total column water vapor
LWC	Liquid water content

REFERENCES

Adler, R. F., and Coauthors, 2003: The version-2 Global Precipitation Climatology Project (GPCP) monthly precipitation analysis (1979–present). *J. Hydrometeor.,* **4,** 1147–1167.

Albrecht, B. A., C. S. Bretherton, D. Johnson, W. H. Schubert, and A. Shelby Frisch, 1995: The Atlantic Stratocumulus Transition Experiment—ASTEX. *Bull. Amer. Meteor. Soc.,* **76,** 889–904.

Anderson, J. L., and Coauthors, 2004: The new GFDL global atmosphere and land model AM2–LM2: Evaluation with prescribed SST simulation. *J. Climate,* **17,** 4641–4673.

Bechtold, P., and Coauthors, 2000: A GCSS model intercomparison for a tropical squall line observed during TOGA-COARE. II: Intercomparison of single-column models and a cloud-resolving model. *Quart. J. Roy. Meteor. Soc.,* **126,** 865–888.

Bony, S., and K. A. Emanuel, 2001: A parameterization of the cloudiness associated with cumulus convection: Evaluation using TOGA COARE data. *J. Atmos. Sci.,* **58,** 3158–3183.

——, and J.-L. Dufresne, 2005: Marine boundary layer clouds at the heart of tropical cloud feedback uncertainties in climate models. *Geophys. Res. Lett.,* **32,** L20806, doi:10.1029/2005GL023851.

——, ——, H. Le Treut, J.-J. Morcrette, and C. Senior, 2004: On dynamic and thermodynamic components of cloud changes. *Climate Dyn.,* **22,** 71–86.

——, and Coauthors, 2006: How well do we understand and evaluate climate change feedback processes? *J. Climate,* **19,** 3445–3482.

Bretherton, C. S., and S. Park, 2009: A new moist turbulence parameterization in the Community Atmosphere Model. *J. Climate,* **22,** 3422–3448.

——, S. K. Krueger, M. C. Wyant, P. Bechtold, E. van Meijgaard, B. Stevens, and J. Teixeira, 1999: A GCSS boundary layer model intercomparison study of the first ASTEX Lagrangian experiment. *Bound.-Layer Meteor.,* **93,** 341–380.

——, J. R. McCaa, and H. Grenier, 2004: A new parameterization for shallow cumulus convection and its application to marine subtropical cloud-topped boundary layers. Part I: Description and 1D results. *Mon. Wea. Rev.,* **132,** 864–882.

Browning, K. A., and Coauthors, 1993: The GEWEX Cloud System Study (GCSS). *Bull. Amer. Meteor. Soc.,* **74,** 387–399.

Cess, R. D., and Coauthors, 1997: Comparison of the seasonal change in cloud-radiative forcing from atmospheric general circulation models and satellite observations. *J. Geophys. Res.,* **102,** 16 593–16 603.

Cheinet, S., and J. Teixeira, 2003: A simple formulation for the eddy-diffusivity parameterization of cloud-topped boundary layers. *Geophys. Res. Lett.,* **30,** 1930, doi:10.1029/2003GL017377.

Chylek, P., U. Lohmann, M. Dubey, M. Mishchenko, R. Kahn, and A. Ohmura, 2007: Limits on climate sensitivity derived from recent satellite and surface observations. *J. Geophys. Res.,* **112,** D24S04, doi:10.1029/2007JD008740.

Collins, W. D., and Coauthors, 2006: The formulation and atmospheric simulation of the Community Atmosphere Model Version 3 (CAM3). *J. Climate,* **19,** 2144–2161.

Colorado State University, cited 2010: BUGS documentation. [Available online at http://kiwi.atmos.colostate.edu/BUGS/.]

Côté, J., S. Gravel, A. Méthot, A. Patoine, M. Roch, and A. Staniforth, 1998: The operational CMCMRB Global Environment Multiscale (GEM) model. Part I: Design considerations and formulation. *Mon. Wea. Rev.,* **126,** 1373–1395.

Cuijpers, J. W. M., and P. Bechtold, 1995: A simple parameterization of cloud water related variables for use in boundary layer models. *J. Atmos. Sci.,* **52,** 2486–2490.

Del Genio, A. D., M. S. Yao, W. Kovari, and K. W. W. Lo, 1996: A prognostic cloud water parameterization for global climate models. *J. Climate,* **9,** 270–304.

Duynkerke, P. G., and J. Teixeira, 2001: A comparison of the ECMWF reanalysis with FIRE I observations: Diurnal variation of marine stratocumulus. *J. Climate,* **14,** 1466–1478.

——, and Coauthors, 1999: Intercomparison of three- and one-dimensional model simulations and aircraft observations of stratocumulus. *Bound.-Layer Meteor.,* **92,** 453–487.

Environmental Modeling Center, 2003: The GFS atmospheric model. National Centers for Environmental Prediction Office Note 442, 14 pp. [Available online at http://www.emc.ncep.noaa.gov/officenotes/newernotes/on442.pdf.]

European Centre for Medium-Range Weather Forecasts, cited 2006: The ECMWF integrated forecast system documentation CY31r1. [Available online at http://www.ecmwf.int/research/ifsdocs/CY31r1/index.html.]

Fowler, L. D., D. A. Randall, and S. A. Rutledge, 1996: Liquid and ice cloud microphysics in the CSU general circulation model. Part 1: Model description and simulated microphysical processes. *J. Climate,* **9,** 489–529.

Gates, W. L., 1992: AMIP: The Atmospheric Model Intercomparison Project. *Bull. Amer. Meteor. Soc.,* **73,** 1962–1970.

Gibelin, A., L. Déqué, and M. Dreveton, 2003: Anthropogenic climate change over the Mediterranean region simulated by a global variable resolution model. *Climate Dyn.,* **20,** 327–339.

Golaz, J.-C., V. E. Larson, and W. R. Cotton, 2002: A PDF-based model for boundary layer clouds. Part I: Method and model description. *J. Atmos. Sci.,* **59,** 3540–3551.

Gu, Y., J. D. Farrara, K. N. Liou, and C. R. Mechoso, 2003: Parameterization of cloud-radiative processes in the UCLA general circulation model. *J. Climate,* **16,** 3357–3370.

Hannay, C., D. L. Williamson, J. J. Hack, J. T. Kiehl, J. G. Olson, S. A. Klein, C. S. Bretherton, and M. Köhler, 2009: Evaluation of forecasted southeast Pacific stratocumulus in the NCAR, GFDL, and ECMWF models. *J. Climate,* **22,** 2871–2889.

Harrison, E. F., P. Minnis, B. R. Barkstrom, V. Ramanathan, R. D. Cess, and G. G. Gibson, 1990: Seasonal variation of cloud

radiative forcing derived from the Earth Radiation Budget Experiment. *J. Geophys. Res.,* **95** (D11), 18 687–18 703.

Hourdin, F., and Coauthors, 2006: The LMDZ4 general circulation model: Climate performance and sensitivity to parametrized physics with emphasis on tropical convection. *Climate Dyn.,* **27,** 787–813.

Huffman, G. J., and Coauthors, 1997: The Global Precipitation Climatology Project (GPCP) combined precipitation dataset. *Bull. Amer. Meteor. Soc.,* **78,** 5–20.

Jakob, C., 1999: Clouds in the ECMWF reanalysis. *J. Climate,* **12,** 947–959.

Janowiak, J. E., A. Gruber, C. R. Kondragunta, R. E. Livezey, and G. J. Huffman, 1998: A comparison of the NCEP–NCAR reanalysis precipitation and the GPCP rain gauge–satellite combined dataset with observational error considerations. *J. Climate,* **11,** 2960–2979.

Johns, T., and Coauthors, 2004: HadGEM1—Model description and analysis of preliminary experiments for the IPCC Fourth Assessment Report. Hadley Centre for Climate Prediction and Research/Met Office Tech. Note 55, 74 pp. [Available online at http://www.metoffice.gov.uk/publications/HCTN/HCTN_55.pdf.]

Juang, H.-M., S. Y. Hong, and M. Kanamitsu, 1997: The NCEP regional spectral model: An update. *Bull. Amer. Meteor. Soc.,* **78,** 2125–2143.

Karlsson, J., G. Svensson, and H. Rodhe, 2008: Cloud radiative forcing of subtropical low level clouds in global models. *Climate Dyn.,* **30,** 779–788.

——, ——, S. Cardoso, J. Teixeira, and S. Paradise, 2010: Subtropical cloud regime transitions: Boundary layer depth and cloud-top height evolution. *J. Appl. Meteor. Climatol.,* **49,** 1845–1858.

Kawai, H., and J. Teixeira, 2010: Probability density functions of liquid water path of marine boundary layer clouds: Geographical and seasonal variations and controlling meteorological factors. *J. Climate,* **23,** 2079–2092.

Khairoutdinov, M. F., D. A. Randall, and C. DeMott, 2005: Simulations of the atmospheric general circulation using a cloud-resolving model as a superparameterization of physical processes. *J. Atmos. Sci.,* **62,** 2136–2154.

Klein, S. A., and D. L. Hartmann, 1993: The seasonal cycle of low stratiform clouds. *J. Climate,* **6,** 1587–1606.

——, and C. Jakob, 1999: Validation and sensitivities of frontal clouds simulated by the ECMWF model. *Mon. Wea. Rev.,* **127,** 2514–2531.

Köhler, M., 2005: Improved prediction of boundary layer clouds. *ECMWF Newsletter,* No. 104, ECMWF, Reading, United Kingdom, 18–22.

Kuwano-Yoshida, A., T. Enomoto, and W. Ohfuchi, 2010: An improved PDF cloud scheme for climate simulations. *Quart. J. Roy. Meteor. Soc.,* **136,** 1583–1597.

Larson, K., D. Hartmann, and S. Klein, 1999: The role of clouds, water vapor, circulation, and boundary layer structure in the sensitivity of the tropical climate. *J. Climate,* **12,** 2359–2374.

Lenderink, G., and A. A. M. Holtslag, 2004: An updated length scale formulation for turbulent mixing in clear and cloudy boundary layers. *Quart. J. Roy. Meteor. Soc.,* **130,** 3405–3427.

Li, J.-L. F., and Coauthors, 2008: Comparisons of satellites liquid water estimates to ECMWF and GMAO analyses, 20th century IPCC AR4 climate simulations, and GCM simulations. *Geophys. Res. Lett.,* **35,** L19710, doi:10.1029/2008GL035427.

Lock, A. P., 2001: The numerical representation of entrainment in parameterizations of boundary layer turbulent mixing. *Mon. Wea. Rev.,* **129,** 1148–1163.

——, A. R. Brown, M. R. Bush, G. M. Martin, and R. N. B. Smith, 2000: A new boundary layer mixing scheme. Part I: Scheme description and SCM tests. *Mon. Wea. Rev.,* **128,** 3187–3199.

Ma, C.-C., C. R. Mechoso, A. W. Robertson, and A. Arakawa, 1996: Peruvian stratus clouds and the tropical Pacific circulation: A coupled ocean–atmosphere GCM study. *J. Climate,* **9,** 1635–1645.

Majewski, D., and Coauthors, 2002: The operational global icosahedral-hexagonal gridpoint model GME: Description and high-resolution tests. *Mon. Wea. Rev.,* **130,** 319–338.

Matsumura, T., M. Ohizumi, H. Kitagawa, and M. Nakagawa, 2002: Outline of the operational numerical weather prediction at the Japan Meteorological Agency-Global Spectral Model (JMA GSM). Japan Meteorological Agency Rep. JMA-GSM0103.

Park, S., C. Deser, and M. A. Alexander, 2005: Estimation of the surface heat flux response to sea surface temperature anomalies over the global oceans. *J. Climate,* **18,** 4582–4599.

Philander, S. G., D. Gu, D. Halpern, G. Lambert, N.-C. Lau, T. Li, and R. C. Pacanowski, 1996: Why the ITCZ is mostly north of the Equator. *J. Climate,* **9,** 2958–2972.

Plummer, D. A., and Coauthors, 2006: Climate and climate change over North America as simulated by the Canadian RCM. *J. Climate,* **19,** 3112–3132.

Potter, G. L., and R. D. Cess, 2004: Testing the impact of clouds on the radiation budgets of 19 AMIP models. *J. Geophys. Res.,* **109,** D02106, doi:10.1029/2003JD004018.

Ramanathan, V., R. D. Cess, E. F. Harrison, P. Minnis, B. R. Barkstrom, E. Ahmad, and D. Hartmann, 1989: Cloud-radiative forcing and climate: Results from the Earth Radiation Budget Experiment. *Science,* **243,** 57–63.

Randall, D. A., and Coauthors, 2003: Confronting models with data. The GEWEX Cloud Systems Study. *Bull. Amer. Meteor. Soc.,* **84,** 455–469.

Rasch, P. J., and J. E. Kristjánsson, 1998: A comparison of the CCM3 model climate using diagnosed and predicted condensate parameterizations. *J. Climate,* **11,** 1587–1614.

Redelsperger, J. L., and Coauthors, 2000: A GCSS model intercomparison for a tropical squall line observed during TOGA-COARE. I: Cloud-resolving models. *Quart. J. Roy. Meteor. Soc.,* **126,** 823–864.

Riehl, H., C. Yeh, J. S. Malkus, and N. E. LaSeur, 1951: The northeast trade of the Pacific Ocean. *Quart. J. Roy. Meteor. Soc.,* **77,** 598–626.

Roeckner, E., and Coauthors, 2003: The atmospheric general circulation model ECHAM5. Part I: Model description. Max-Planck-Institut für Meteorologie Rep. 349, 127 pp.

Rossow, W. B., and R. A. Schiffer, 1991: ISCCP cloud data products. *Bull. Amer. Meteor. Soc.,* **72,** 2–20.

——, and ——, 1999: Advances in understanding clouds from ISCCP. *Bull. Amer. Meteor. Soc.,* **80,** 2261–2287.

Saha, S., and Coauthors, 2006: The NCEP climate forecast system. *J. Climate,* **19,** 3483–3517.

Schmidt, G. A., and Coauthors, 2006: Present-day atmospheric simulations using GISS Model-E: Comparison to in-situ, satellite, and reanalysis data. *J. Climate,* **19,** 153–192.

Siebesma, A. P., and J. Teixeira, 2000: An advection-diffusion scheme for the convective 647 boundary layer: Description and 1D results. Preprints, *14th Symp. on Boundary Layers and Turbulence,* Aspen, CO, Amer. Meteor. Soc., 133–136.

——, and Coauthors, 2003: A large-eddy simulation intercomparison study of shallow cumulus convection. *J. Atmos. Sci.,* **60,** 1201–1219.

——, and Coauthors, 2004: Cloud representation in general circulation models over the northern Pacific Ocean: A EUROCS intercomparison study. *Quart. J. Roy. Meteor. Soc.,* **130,** 3245–3267.

Slingo, J. M., 1980: A cloud parameterization scheme derived from GATE data for use with a numerical model. *Quart. J. Roy. Meteor. Soc.,* **106,** 747–770.

——, 1987: The development and verification of a cloud prediction scheme in the ECMWF model. *Quart. J. Roy. Meteor. Soc.,* **113,** 899–927.

Soares, P. M. M., P. M. A. Miranda, A. P. Siebesma, and J. Teixeira, 2004: An eddy-diffusivity/mass-flux scheme for dry and shallow convection. *Quart. J. Roy. Meteor. Soc.,* **130,** 3365–3384.

Stephens, G. L., 2005: Cloud feedbacks in the climate system: A critical review. *J. Climate,* **18,** 237–273.

——, and Coauthors, 2002: The *CloudSat* mission and the EOS constellation: A new dimension of space-based observations of clouds and precipitation. *Bull. Amer. Meteor. Soc.,* **83,** 1771–1790.

——, and Coauthors, 2008: *CloudSat* mission: Performance and early science after the first year of operation. *J. Geophys. Res.,* **113,** D00A18, doi:10.1029/2008JD009982.

Steppeler, J., G. Doms, U. Schättler, H. W. Bitzer, A. Gassmann, U. Damrath, and G. Gregoric, 2003: Meso-gamma scale forecasts using the nonhydrostatic model LM. *Meteor. Atmos. Phys.,* **82,** 75–96.

Stevens, B., and Coauthors, 2001: Simulations of trade wind cumuli under a strong inversion. *J. Atmos. Sci.,* **58,** 1870–1891.

Stubenrauch, C. J., W. B. Rossow, F. Chéruy, A. Chédin, and N. A. Scott, 1999: Clouds as seen by satellite sounders (3I) and imagers (ISCCP). Part I: Evaluation of cloud parameters. *J. Climate,* **12,** 2189–2213.

Teixeira, J., 1999: The impact of increased boundary layer vertical resolution on the ECMWF forecast system. ECMWF Tech. Memo. 268, 55 pp.

——, and T. F. Hogan, 2002: Boundary layer clouds in a global atmospheric model: Simple cloud cover parameterizations. *J. Climate,* **15,** 1261–1276.

——, P. May, M. Flatau, and T. F. Hogan, 2008: On the sensitivity of the SST from a global ocean–atmosphere coupled system to the parameterization of boundary layer clouds. *J. Mar. Syst.,* **69,** 29–36.

Tiedtke, M., 1993: Representation of clouds in large-scale models. *Mon. Wea. Rev.,* **121,** 3040–3061.

Tompkins, A. M., 2002: A prognostic parameterization for the subgrid-scale variability of water vapor and clouds in large-scale models and its use to diagnose cloud cover. *J. Atmos. Sci.,* **59,** 1917–1942.

Uppala, S. M., and Coauthors, 2005: The ERA-40 Re-Analysis. *Quart. J. Roy. Meteor. Soc.,* **131,** 2961–3012.

van Meijgaard, E., L. H. van Ulft, W. J. van den Berg, F. C. Bosveld, B. J. J. M. van den Hurk, G. Lenderink, and A. P. Siebesma, 2008: The KNMI regional atmospheric climate model RACMO, version 2.1. KNMI Tech. Rep. 302, 43 pp.

von Engeln, A., J. Teixeira, J. Wickert, and S. Buehler, 2005: Using CHAMP radio occultation data to determine the top altitude of the planetary boundary layer. *Geophys. Res. Lett.,* **32,** L06815, doi:10.1029/2004GL022168.

von Salzen, K., N. A. McFarlane, and M. Lazare, 2005: The role of shallow convection in the water and energy cycles of the atmosphere. *Climate Dyn.,* **25,** 671–688.

Webb, M., C. Senior, S. Bony, and J.-J. Morcrette, 2001: Combining ERBE and ISCCP data to assess clouds in the Hadley Centre ECMWF and LMD atmospheric climate models. *Climate Dyn.,* **17,** 905–922.

Wentz, F. J., 1997: A well-calibrated ocean algorithm for SSM/I. *J. Geophys. Res.,* **102** (C4), 8703–8718.

Wielicki, B. A., R. D. Cess, M. D. King, D. A. Randall, and E. F. Harrison, 1995: Mission to planet earth: Role of clouds and radiation in climate. *Bull. Amer. Meteor. Soc.,* **76,** 2125–2153.

Wood, R., and C. S. Bretherton, 2004: Boundary layer depth, entrainment, and decoupling in the cloud-capped subtropical and tropical marine boundary layer. *J. Climate,* **17,** 3576–3588.

——, and ——, 2006: On the relationship between stratiform low cloud cover and lower-tropospheric stability. *J. Climate,* **19,** 6425–6432.

Wyant, M. C., C. S. Bretherton, H. A. Rand, and D. E. Stevens, 1997: Numerical simulations and a conceptual model for the stratocumulus to trade cumulus transition. *J. Atmos. Sci.,* **54,** 168–182.

——, ——, J. Bacmeister, J. Kiehl, I. Held, M. Zhao, S. Klein, and B. Soden, 2006: A comparison of low-latitude cloud properties and their response to climate change in three AGCMs sorted into regimes using mid-tropospheric vertical. *Climate Dyn.,* **27,** 261–279.

Zhang, M. H., and Coauthors, 2005: Comparing clouds and their seasonal variations in 10 atmospheric general circulation models with satellite measurements. *J. Geophys. Res.,* **110,** D15S02, doi:10.1029/2004JD005021.

Zhong, A., R. Colman, N. Smith, M. Naughton, L. Rikus, K. Puri, and F. Tseitkin, 2001: Ten-year AMIP-1 climatologies from versions of the BMRC atmospheric model. BMRC Research Rep. 83, 34 pp.